

CZECH TECHNICAL UNIVERSITY IN PRAGUE

FACULTY OF CIVIL ENGINEERING

DEPARTMENT OF GEOMATICS



Master' s Thesis

**Comparison of Classification of the Burnt Class in the Temporal
Development from the Sentinel-2 Data with the CORINE System
Classes**

Bc. LUCIE DĚKANOVÁ

Supervisor: Prof. Ing. Lena Halounová, CSc.

Study Programme: Geodesy and Cartography

Field of Study: Geomatics

2021

ZADÁNÍ DIPLOMOVÉ PRÁCE

I. OSOBNÍ A STUDIJNÍ ÚDAJE

Příjmení: Bc. Děkanová Jméno: Lucie Osobní číslo: 468200
 Zadávající katedra: geomatiky
 Studijní program: Geodézie a kartografie
 Studijní obor: Geomatika

II. ÚDAJE K DIPLOMOVÉ PRÁCI

Název diplomové práce: Porovnání klasifikace třídy spáleníšť v časovém vývoji z dat družic Sentinel-2 s třídami CORINE systému

Název diplomové práce anglicky: Comparisom of classification of the burnt class in the temporal development from the Sentinel-2 data with the CORINE system classes

Pokyny pro vypracování:

- 1) Vybrat vhodné území z družicových dat Sentinel 2A, 2B, kde se dle CORINE vyskytují významné plochy spáleníšť
- 2) Vybrat bezoblačné scény družic Sentinel-2 od roku 2015 do 2020 ze začátku podzimního období
- 3) Vypočítat dodatečné vhodné kanály ze vstupních dat pro klasifikace
- 4) Vybrat trénovací plochy pro klasifikaci a testovací plochy pro určení přesnosti klasifikace
- 5) Posoudit příznakový prostor vybraných trénovacích ploch pro klasifikace.
- 6) Provést klasifikace a vyhodnotit jejich přesnost
- 7) Porovnat klasifikované plochy spáleníšť s daty CORINE a určit shodu a rozdíly.
- 8) Provést rozbor shod a rozdílů

Seznam doporučené literatury:

- 1) PATRONO, Andrea; BAPTISTA, Adriano; EBELTJES, Jan. Multitemporal LANDSAT TM data for monitoring the effects of forest fires and vegetation recovery processes in the Mediterranean areas. ISPRS Archives 2000. [Online]. Available at: https://www.isprs.org/proceedings/XXXIII/congress/part7/1131_XXXIII-part7.pdf
- 2) GALLAUN, Heinz; BANNINGER, Cliff. Monitoring fire – affected wildlands in the Mediterranean region by applying a remote sensing and GIS approach. ISPRS archives 1996. [Online]. Available at: https://www.isprs.org/proceedings/XXXI/congress/part7/240_XXXI-part7.pdf
- 3) NIOTI, Foula ; XYSTRAKIS, Fotios ; KOUTSIAS, Nikos; DIMOPOULOS, Panayotis. A Remote Sensing and GIS Approach to Study the Long-Term Vegetation Recovery of a Fire-Affected Pine Forest in Southern Greece. Remote Sens. 2015, 7(6), 7712-7731. [Online]. Available at: <https://www.mdpi.com/2072-4292/7/6/7712/htm>

Jméno vedoucího diplomové práce: prof. Ing. Lena Halounová, CSc.

Datum zadání diplomové práce: 15. 2. 2021 Termín odevzdání diplomové práce: 17. 5. 2021
Údaj uveďte v souladu s datem v časovém plánu příslušného ak. roku

.....
 [Redacted Signature]

Podpis vedoucího práce

.....
 [Redacted Signature]

Podpis vedoucího katedry

III. PŘEVZETÍ ZADÁNÍ

Beru na vědomí, že jsem povinen vypracovat diplomovou práci samostatně, bez cizí pomoci, s výjimkou poskytnutých konzultací. Seznam použité literatury, jiných pramenů a jmen konzultantů je nutné uvést v diplomové práci a při citování postupovat v souladu s metodickou příručkou ČVUT „Jak psát vysokoškolské závěrečné práce“ a metodickým pokynem ČVUT „O dodržování etických principů při přípravě vysokoškolských závěrečných prací“.

.....
 [Redacted Signature]

Datum převzetí zadání

.....
 [Redacted Signature]

Podpis studenta(ky)

Declaration

I hereby declare that this Master's thesis entitled "*Comparison of Classification of the Burnt Class in the Temporal Development from the Sentinel-2 Data with the CORINE System Classes*" represents my own ideas and words. Furthermore, I declare that I have been working on it independently and I have listed all the publications and literature, which had been used.

Date:

.....

Bc. Lucie Děkanová

Acknowledgements

I would like to express my special thanks to my supervisor Prof. Ing. Lena Halounová, CSc. for her guidance, providing necessary information regarding the topic as well as her willingness to share her vast knowledge, which helped me to complete this thesis.

ABSTRACT

This Master's thesis focuses on the methods that could be applied for detection and following analysis of burnt areas using Sentinel-2 data. The main purpose of this study is to compare the burnt areas differentiated by the supervised classification during the 5 years with the CORINE system classes as well as to show the spectral evolution of the land cover affected by fires.

KEY WORDS

Remote sensing, Sentinel-2, QGIS, CORINE, Supervised Classification, Atmosphere Resistant Vegetation Index, Normalized Difference Vegetation Index, Normalized Burn Ratio

ABSTRAKT

Tato diplomová práce je zaměřena na metody, které lze využít k detekci a analýze spálenišť pomocí dat družic Sentinel-2. Hlavním cílem této práce je porovnání klasifikovaných spálenišť pomocí řízené klasifikace v pětiletém období s třídami CORINE systému a zobrazit časový vývoj půdního krytu zasaženého požáry.

KLÍČOVÁ SLOVA

Dálkový průzkum Země, Sentinel-2, QGIS, CORINE, řízená klasifikace, ARVI, NDVI, NBR

Table of Contents

List of Abbreviations.....	9
Introduction.....	10
Aims of thesis.....	11
1 Research.....	12
2 Methodology.....	23
2.1 Area.....	23
2.1.1 Location.....	24
2.1.2 Climate and Vegetation.....	25
2.2 Data.....	26
2.2.1 Raster Data: Sentinel-2.....	26
Product Types.....	27
Spectral Bands.....	27
Imagery used.....	29
Products.....	31
Level-1C Product.....	31
Level-2A Product.....	32
Selecting the Seasons and Years.....	32
Choosing the Signature Space.....	32
Normalized Difference Vegetation Index (NDVI).....	34
Atmospherically Resistant Vegetation Index (ARVI).....	34
Normalized Burn Ratio (NBR).....	35
2.2.2 Vector Data: CORINE Land Cover.....	36
Burnt Areas.....	37
2.3 Image Processing.....	38
2.3.1 Classification.....	38

2.3.2 Supervised Classification.....	39
Maximum Likelihood	40
Classification Process.....	40
Training set.....	41
Selection of the Test Areas	43
Accuracy Assessment.....	43
2.4 Temporal Development	46
2.4.1 Selection of Burnt Areas.....	46
2.4.2 Comparison.....	46
Comparison with CLC	47
Comparison with classified Burnt Areas.....	48
2.4.2 Selection of the Areas to be analyzed	49
Division of the Burnt Areas	49
Selection of the Forested Areas untouched by fires.....	51
2.4.3 Computation of dNBR	51
2.4.4 Statistical Evaluation	52
2.5 Software.....	53
2.5.1 QGIS	53
Semi-Automatic Classification Plugin.....	53
2.5.2 GRASS.....	54
QGIS with GRASS	54
3 Results.....	55
3.1 Classification Results	55
3.2 Temporal Development Results	62
3.2.1 Transitional woodland-shrub	62
3.2.2 Coniferous forests	72
3.2.3 Mixed Forests	77

3.2.4 Sclerophyllous Vegetation.....	84
Discussion	88
Conclusion	89
References	91
List of Figures	95
List of Tables.....	97
Attachments.....	98

List of Abbreviations

NDVI	Normalized Difference Vegetation Index
ARVI	Atmospherically Resistant Vegetation Index
NBR	Normalized Burn Ratio
dNBR	Differenced Normalized Burn Ratio
SAVI	Soil-adjusted Vegetation Index
MSAVI	Modified Soil Adjusted Vegetation Index
CBI	Composite Burn Index
BSI	Bone Scan Index
USGS	United States Geological Survey
ASTER	Advanced Spaceborne Thermal Emission and Reflection Radiometer
GDEM	Global Digital Elevation Model
DEM	Digital Elevation Model
CLC	CORINE Land Cover
ESA	European Space Agency
ESOC	European Space Operations Centre
ISP	Instrument Source Packet
TOA	Top of Atmosphere
BOA	Bottom of Atmosphere
ROI	Region of Interest

Introduction

There is no doubt that forests are one of the most important parts of the Earth's vegetation. During the last two decades, forests have been facing enormous deforestation. This decrease of forest areas has both a human and natural origin. One of the important natural factors causing deforestation is fire, which appears in various types of forests worldwide.

Millions of hectares of forests all over the world are burned every year. Satellite remote sensing can be used as a great source describing the damage and recovery process of the areas affected by the fire. It is well-known that satellite data have been used to monitor areas affected by fires. Nowadays, there is an increasingly greater need to improve post-fire detection using satellite data because of the climate changes, which bring a greater and more frequent risk of natural hazards and related disasters in the whole world.

As a part of the project “*Geo-harmonizer: EU-wide automated mapping system for harmonization of Open Data based on FOSS4G and Machine Learning*“ [1], this thesis deals with the burnt areas detection in the Mediterranean forest land cover, where fires occur the most in comparison with the rest of the European vegetation.

Supervised classification of the satellite multispectral Sentinel-2 data could take a big part in the detection of the burnt areas. In this thesis, one of the main goals is to find a suitable combination of the raster bands for the following classification. Due to this fact, the research related to forest fire detection has been done and additional indices were included in the classification and for future analysis.

These indices are used for the supervised classification as well as for the graphical representation. The final analysis is primarily based on the spectral changes of the burnt areas (both pre and post-fire) and their homogenous surroundings. This spectral evolution of the land cover is done through multitemporal analysis from 2015 until 2020.

Aims of thesis

The main goal of this paper is to detect burnt areas in temporal development. In this thesis, Sentinel-2 data and CORINE Land Cover classes will be used.

The burnt area class obtained by classification from Sentinel-2 data is going to be compared to the CORINE Land Cover's Burnt Area class. It will be determined whether the burnt areas classified from the satellite data are depicted in the CLC Burnt Area class or not, and if so, in what type of vegetation they appear and for how long the burnt areas classified from the Sentinel-2 images can be distinguished in CLC.

Even though numerous studies have already focused on the extraction of the burnt areas using spectral indices, there still could be many other options for using them more effectively and in an easier way when detecting burnt areas.

The following problem statements and investigation topics will be considered in this thesis:

- 1) Choosing a suitable area based on the frequency and severity of the forest fires occurring on the land – selecting bands and indices with references to the bibliography
- 2) Determining the selection of the seasons and years for providing analysis of temporal development
- 3) Proposing methodology for the analysis and following evaluation according to the research
- 4) Comparing the classified areas with the areas specified in CORINE Land Cover
- 5) Evaluating the temporal development in the different types of vegetation

1 Research

As said before, forest fires are a major issue, which affects various types of vegetation. During the last few decades, the number of forest fires has been increasing so there is an important reason to continue to find new methods for burnt area analysis. Due to this fact, the research on past studies dealing with fire detection has been drawn up.

This research is mainly based on the methods of pre and post-fire detection using satellite data. Regarding the information acquired, studies related to this topic have been the subject of examination since the late 1980s.

Thanks to gradual development of the satellite data, there are more and more resources that can be used for analysis. Nowadays, we can use a lot of resources to take advantage of. The text below brings a list of cases, which were used for the thesis and its aims.

Case 1 - Forest fires in Portugal

One of the most crucial resources for this thesis is a study “*Detection of changes in forest landcover type after fires in Portugal*” whose primary goal is to detect the changes in the forest landcover type after fires in Portugal using the Atmosphere Resistant Vegetation Index. The ARVI images from the year before the fire are compared to the images obtained two years post-fire and the differenced image is computed. Thanks to this, the burnt area could be analyzed.

The study lasted from 1990 to 1998. A single Landsat TM image from spring and summer from each year was required. The methodology is based on a spectral change identification technique using vegetation index differencing.

This article shows that the ARVI for the regrowth of vegetation is higher than for burnt areas. The mean value and standard deviation are computed from the ARVI differenced image.

For the change of spectral analysis, the land cover is analyzed for test areas. In order to regard the spectral evolution of the land cover over forest areas, 5 types of test areas are recognized: Shrubland-Shrubland (Sh-Sh), Eucalyptus-Eucalyptus (Eu-Eu), Pine-

Shrubland (Pi-Sh), and Pine-Eucalyptus (Pi-Eu). The last test area type was divided into two different sub-types in the first (Pi-Eu-92) or the second year (Pi-Eu-93) after the fire.

In conclusion, the study indicates that the regrowth of the shrubland and pine is slower in comparison with the regrowth of the Eucalyptus.[2]

Case 2 - Forest fires in Greece 2016

The next useful study “*Evaluating and comparing Sentinel-2A and Landsat-8 Operational Land Imager (OLI) spectral indices for estimating fire severity in a Mediterranean pine ecosystem of Greece*” [3] compares 3 fire severity indices (CBI, Geometrically structured CBI, weighted CBI) and spectral indices derived from Sentinel-2A and Landsat 8. In the study they use Normalized Difference Vegetation Index, Normalized Burn Ratio, differenced Normalized Burn Ratio, differenced Normalized Difference Vegetation Index and 7 Sentinel-2A specific indices. It focuses on the pre and post-fire September 2016. The study used Landsat 8 images processed for L1T terrain and Sentinel-2A images processed to Level L1C (both acquired in August and September 2016).

The sample plots were chosen 3 weeks after the fires and randomly selected areas, which were placed within Calabrian pine dominated areas characterized by 4 levels of burn severity – unburned, low severity, moderate severity, and high severity. At the center point of each area, digital photos were taken, and the Global Navigation Satellite System coordinates were recorded. There were four identified strata (substrate, herbs and low shrubs, tall shrubs and low trees, and tall trees). For each stratum, the fire severity was assigned a value from 0 to 3 (as described in CBI). The final CBI value of severity was calculated by combining the strata values of each area.

The results of the analysis of the separability demonstrate that in case of the spectral response over the electromagnetic spectrum in both sensors, the lowest separability was found in blue to red spectral bands of the post-fire images, with the green band presents both in Sentinel (0.20) and Landsat (0.30) higher values.

The first red edge band of Sentinel (B5) shows a low separability value while the wide NIR (B8) and the two narrow NIR (B7 and B8A) bands (NIR shoulder) indicate more

efficient discrimination of burned-unburned areas thanks to their sensitivity in the reflectance of leaf pigments and ash deposition.

Landsat-based spectral indices indicate higher values of separability unlike the indices generated from Sentinel. The dNBR had a higher separability value compared to the wider NIR band (B8).

The results showed that the dNBR is slightly more able to estimate field-based fire severity data in comparison to the other examined spectral indices that are mainly reported in the most remotely sensed estimation of fire and burn severity worldwide.[3]

Case 3 - Forest fires in Greece 1991-1999

The paper “*Multitemporal LANDSAT TM data for monitoring the effects of forest fires and vegetation recovery processes in the Mediterranean areas*” describes uses of Landsat TM bands for vegetation discrimination. The study lasted from 1991 until 1999.

Each selected band is used for getting particular information:

- TM band 4 (post-fire imagery) - for highlighting the areas affected by fires
- TM band 7, band 4, band 1 (post-fire imagery) - the extent of fires in RGB color
- multi-temporal RGB color to detect spectral changes (pre-fire, immediately post-fire and the following year in spring).

Thanks to the DN (Digital Number) values, the burnt areas are identified.

The next step is to find out the burnt areas in the pre-fire imagery. This is done to study relations between the original vegetation and the natural re-growth rates. The first several classes are recognized thanks to their different combinations of digital values (based on their inherent spectral reflectance). The training samples are identified, and a numerical description of the spectral attributes of each land cover type is developed (the land cover maps were available). The categorization of every pixel in the image data is carried out using the Maximum Likelihood algorithm.

The supervised classification is being applied (pre-fire images). Landsat TM band 3 is significant for discriminating the vegetation types (the chlorophyll absorption range), TM band 4 to determine veg. types, health, and biomass content, TM band 5 gives a good contrast among vegetation types. The color composites derived from these bands help to determine training samples.

For the monitoring of the vegetation condition, the NDVI was used. Vegetated areas show high values thanks to their high NIR reflectance and low red reflectance. Rock and bare soil have similar reflectance in the two bands, the result is near 0.

The differences among NDVI images of successive years were used to observe the recovery of the vegetation. The different images were classified with an unsupervised statistical method to group and map areas showing homogeneous differences of NDVI values.

The growth model was determined after the NDVI averages were computed. Using the latest NDVI, the future of the vegetation could have been forecasted.

As a result, the easiest solution could be the 7-4-1 TM band combination of the immediate post-fire image, in RGB using the PCI. This process was followed by masking and raster to polygon operations to create an area of interest to focus on the next part of the analysis.

In the case of monitoring and modeling vegetation growth, the NDVI values reached pre-fire levels in an average of 2 or 3 years. The unsupervised classification of the NDVI differences was done to identify and group zones with homogeneous growth rates. It was computed that in a few areas, the activity was higher than in the pre-fire times.[4]

Case 4 - Forest fires in Spain

In "*Modeling rates of ecosystem recovery after fires by using Landsat TM data*", nine Landsat images from 1984 to 1994 are used. The landscape is separated into units depending on their spatial patterns of types of shrubs. There are three types of differentiated vegetation types: sparse shrubs, dense shrubs, and trees plus shrubs.

The degree of photosynthetic activity is examined using the NDVI and the differences in humidity conditions by the infrared region in the Landsat TM5 band.

Firstly, imagery is converted into apparent reflectance by sensor calibration coefficients. To minimize the effect of the atmosphere, an empirical atmospheric normalization is performed. The reference image is used to normalize multitemporal data sets regarding another reference image (image with the lowest contribution of atmospheric reflectance). A selection of pseudo-invariant pixels is chosen from each TM scene.

The topographic effect (TM data) is corrected by the Minnaert Method. To compute angles, DMT was used (1:10 000 scales). It is evaluated for each different TM band (because of the wavelength difference).

The areas affected by fires (during 1984-85) are masked to avoid the selection of the wrong training areas (areas with repetitive fires during the observation period) to get the post-fire period to be as long as possible. The annual maps of burnt land for the multitemporal series analyzed are performed.

For the comparison, the fire masks are taken from 3 NDVI images that correspond one year before the fire and 2 years post-fire. The difference between the first year and the second year after the fire is also considered to determine the regenerative process of vegetation.

In the end, a multitemporal unsupervised classification is done to mask the burned lands each year. To verify the accuracy of the classification, aerial photos are used.

As a result, the vegetation after the fire (1989) is in a similar condition as before the fire.[5]

Case 5 -Forest fires in Greece

Another method that should be mentioned is described in “*Monitoring fire – affected wildlands in the Mediterranean region by applying a remote sensing and GIS approach*”. This method was applied on imagery from the late 1980s and uses the Modified Soil Adjusted Vegetation Index (MSAVI).

For the estimation of the vegetation cover, the areas without any vegetation and forested sites are used. No burned sites are chosen. The pine forests are used as a reference for forested sites. The MSAVI values are compared to ground-acquired vegetation cover data for 39 reference areas. To check the quality, 14 validation sites, in addition, are appended.

For the evaluation of the extent of regeneration, the difference in vegetation cover between the two image acquisition dates is applied. The datasets had to be georeferenced.

The potential of natural regeneration after a fire depends on the availability of water for plant regrowth in the dry period. Deep soils store more water and carry denser vegetation. Since the correlation between MSAVI and vegetation cover is high, values delivered using MSAVI from imagery acquired in the dry period can be used to estimate the water storage capacity. But it can be used only if the area has not been affected by fires for a long time. The accuracy was assessed by comparing the PNR estimates for the 14 validation sites.

The risk of soil erosion in a burning forest was computed using the slope length exponent, topographic factor, slope, slope length.

For calculating the risk of desertification, the combination of the potential of natural regeneration and the risk of soil erosion was used. It was divided into five classes, with values going from a minimum of 2 (without any risk) for 1 class, to a maximum of 10 (very high risk) for class 5.

The result of this study gives a possibility of how to monitor and map land cover and related changes over geographical areas. [6]

Case 6 - Forest fires in Italy

The next study “*On the Use of Satellite Sentinel-2 Data for Automatic Mapping of Burnt Areas and Burn Severity*” focuses on the pre and post-fire analysis of the fire, which took place in August 2017 in Italy.

The main purpose is to develop a model that can automatically detect the burned areas using Sentinel-2 data using NBR and dNBR.

The dNBR maps should highlight the burnt areas, characterize burn severity levels, and provide indications of the changes induced by fire.

To overcome the disadvantage of the fixed threshold values, one of the most effective ways to inform about the effects of fire, is to use a statistical analysis: Moran, Getis-Ord, and Geary to enhance fire severity levels. In this study, these three analyses were used to compare their effectivity.

The local indicators provide a new image with a value of the autocorrelation for each pixel. They can identify discrete spatial patterns. These indicators show a different concept of spatial association:

- Local Moran's I: a high value of the index means positive correlation both for high values and for low values of intensity;
- Local Geary's C: detects areas of differences between events;
- Getis and Ord's Gi: a high value of the index means a positive correlation for high values of intensity, while a low value of the index means a positive correlation for low values of intensity.

In this study, the dNBR maps and the classification from the different LISA indices are observed to categorize the burn severity levels without using a fixed threshold. The K-means algorithm is used.

The dNBR map is analyzed from the difference between pre and post-fire indices. After the analysis, it is discovered that some of the computed values don't fit. Because of this, the classification needed to be improved. The unsupervised classification based on K-means is applied to dNBR and to the outputs of LISA, Getis-Ord's Gi, Geary, and Moran obtained from dNBR.

The outputs from the classification of the Getis-Ord Gi, Geary are not able to capture the burn severity and are also affected by commission errors. Moran is able to better discriminate fire-affected from unaffected areas and to reliably characterize burn severity.[7]

Case 7 - Forest fires in Turkey

Another study named “*Assessment of Fire Severity and Post-Fire Regeneration based on Topographical Features using Multitemporal Landsat Imagery: A CASE STUDY in MERSIN, TURKEY*” aims their attention to fire severity and post-fire regeneration. In the study, they use a total of 4 Landsat ETM+ images obtained from the USGS archives. One pre-fire image was obtained on 7th April 2008 and 3 post-fire images on 14 September 2008, 19th June 2011, and 13th July 2014. All of the images are geometrically corrected and resampled.

To produce the DEM, the ASTER GDEM is used. All analyses for determining burn severity and vegetation regeneration are carried out using ERDAS IMAGINE (2013) and ArcGIS (v. 10.0) software packages.

For the mapping of burn severity, the NBR is calculated from pre and post-fire ETM+ scenes. After that, the pre and post-NBR ratios are differenced to calculate burn severity.

The detailed overview of dNBR values demonstrates that positive values show an decrease in vegetation, that negative shows an increase.

The post-fire regeneration analysis is performed on the multitemporal analysis of the NDVI and SAVI images. NDVI values range from -1 to +1, where low values (0.1 and below) show the absence of vegetation and high values (0.6 to 1) indicate dense and healthy vegetation. The SAVI was applied to estimate vegetation regrowth rates.

The analysis of vegetation regeneration demonstrates that vegetation cover has recovered to around 60% of the pre-fire levels after 6 years according to NDVI-SAVI multitemporal validation. Post-fire SAVI spatial patterns show a relatively rapid regeneration compared to NDVI. The use of SAVI to determine post-disturbance recovery could be an alternative to NDVI.

The recovery of the vegetation is better on north-facing slopes compared to south-facing slopes (related to northern hemisphere dynamics). This is investigated using ASTER GDEM.[8]

Case 8 - Forest fires in Australia

Last but not least, the study “*A Remote Sensing Approach to Mapping Fire Severity in South-Eastern Australia using Sentinel-2 and Random Forest*” zeroes in on finding out the fire severity in Australian forests. Eight fires (in variable types of climate zones – temperate, Mediterranean, subtropical, semi-arid zones) are selected based on the availability of high-resolution 4-band (B, G, R, NIR) post-fire digital aerial photos.

To generate digitalized spatial polygons of homogenous sample areas of fire severity classes, the Aerial Photograph Interpretation is used. The classification of severity is done in ArcMap 10.4, producing five severity classes based on levels of vegetation scorch and consumption of canopy and understory layers. These layers are used to determine various degrees and post-fire changes of biomass and foliage cover, woodlands, shrubs - with strong correlations and field based measures of fire severity. This classification was introduced by *Hudak et al., McCarthy et al, Collins et al.*

Random sampling points are generated in polygons of Aerial Photograph Interpretation severity classes. The generated number of sampling points is as large as possible while being randomly distributed and representative of the real-world occurrences of fire severity classes in each fire. For every sampling point in each fire, corresponding pixel values are extracted for each candidate fire severity index using the raster and shapefile packages in R.

Then, the Sentinel-2 imagery (low cloud cover), which is close to the start and end date of each fire, is selected. The Sentinel-2 SWIR bands were pan-sharpened to 10m resolution. To fit a local linear relationship between each low-resolution SWIR band and the high-resolution red band using the pixels in a 7 by 7 window, a robust regression technique was used.

The band pixels with a low resolution are recalculated to ones with a higher resolution using the local regression model. The 10 m surface reflectance images are recombined into a single stack of Sentinel-2 bands at 10 m resolution that corresponds to the equivalent Landsat TM bands (B, G, R, NIR, SWIR1, SWIR2).

In the study, they try a lot of candidate fire severity indices computed from the bands mentioned above. They conclude that the BSI classification is not useful for fire severity classification.

Previous studies indicate dNBR is better than differenced NDVI for fire severity classification (Veraverbeke et al., 2010; Collins et al., 2018). However, these reflectance-based indices are included because they are the closest analogous reflectance-based indices to the fractional cover indices of change in bare cover and change in total vegetative cover.

Random forest modeling generates an ensemble of regression trees, through a bootstrap aggregated sampling of training data. At each node in a decision tree, a random selection of predictor variables is evaluated for their ability to split training data into response classes, with the variable leading to the most homogeneous classification being selected. The models are compared for each candidate severity index: for each fire, in combination, and for all fires. This is done to test the model for further processing.

Then, the effect of the landscape on Random forest is being examined. The limitations of classification are the dense canopy, shadow cast by steep slopes, or rugged terrain. The goal is to quantify their effect on the classification.

Foliage Projective Cover, an indicator of long-term canopy density (robust to seasonal variation), is developed from a model, calibrated to ground-based measurements using fractional cover transects, and validated against LiDAR data.

A high-resolution version of Foliage Projective Cover developed by Fisher et al. (2016) is used, calculated from SPOT5 satellite imagery across four consecutive summers (2008–2011).

The Terrain Ruggedness Index is a standard index defined as the mean difference between a central pixel and its surrounding cells (Wilson et al., 2007). This index is derived from the 1s Shuttle Radar Topography Mission, Digital Elevation Model.

The differences in community structure can also affect the fire severity indices. Because of that, the analysis is restricted to dry sclerophyll forests.

Regarding the results, time series plots for the Sir Ivan Fire show greater separation between pre and post-fire pixel values with increasing severity for NBR, bare fractions, and green cover fractions. The other studied fires demonstrate the same trends in NBR and fractional cover pixel values. The comparison of each fire severity index shows the comparable accuracy of each fractional cover index to each reflectance-based index. There is a consistent trend of increasing Kappa scores and balanced accuracy with models that included at least one of the NBR-based indices with at least one of the fractional cover-based indices.[9]

Conclusion

For the purpose of this thesis, it was decided to use NDVI, ARVI and NBR indices for the pre and post-fire analysis. As emerged from the research, all three indices can be applied to estimate vegetation regrowth rates. It can be used to compute the fire severity, and they can be used as an alternative to each other plus their computation is not an exacting task, which is a great benefit. All these indices are the vegetation indices and they are all computed using NIR wavelengths.

2 Methodology

In this chapter, the methodology will be described.

2.1 Area

As a first step, a suitable area to be analyzed was selected. The area of interest was chosen in the European territory.

In the beginning, an area of frequent occurrence of forest fires had to be chosen. The selection was executed using **CORINE Land Cover** vector layers and **Sentinel Playground** (<https://apps.sentinel-hub.com/sentinel-playground>).

The CLC was downloaded from the website (<https://land.copernicus.eu/pan-european/corine-land-cover>). The selection of the analyzed burnt areas was done based on the available CLC layers from 2000, 2006, 2012, and 2018.

Once the data was available, the layers were visually compared with each other, and the places with frequent fires were picked. Following the thoroughgoing comparison, the Iberian Peninsula was considered to be the most fire-affected area in the whole of Europe.

Afterward, it was determined if the burnt area class from the CLC 2012 or CLC 2018 was distinguishable in the Sentinel-2 data from 2015. It was done using the Sentinel Playground browser. For the recognition of the burnt areas, the satellite image was displayed in infrared color (displayed in NIR, R, and B). This band combination was chosen because of its use for vegetation detection and its great recognition of burnt areas. The vegetation emerges in the shades of red, soils from dark to light browns, and urban areas are visible in yellow or gray. Burnt areas appear in black, dark grey, or brown.

It was found out that the burnt area class from CLC 2012 was no longer visible in the satellite images from 2015. However, one area demonstrated in the CLC 2018 was still noticeable in the satellite image from 2015.

After that, six vector layers were created in QGIS. These layers showed the burnt areas determined in the CORINE Land Cover with a minimum 6-year period (intersection of 2000 and 2006, 2006 and 2012, 2012 and 2018), 12-year period (2000 and 2012, 2006 and 2018), and 18-year period (2000 and 2018). The CLC class of burnt areas needed to be selected from the whole vector CLC layer. It was carried out by the *Extract by Attribute* function in QGIS. Then, the intersection of each pair of years was done by the *Intersect* function.

According to the results of the intersection, it was concluded that no same burnt areas from each CORINE Land Cover were registered in the others. It signifies that the full regeneration of the forested areas (defined in CLC) affected by fires lasts for less than six years.

After the careful analysis using CORINE Land Cover, the place with frequent forest fires in the Mediterranean forest vegetation had been found.

2.1.1 Location

The study area is located on the Portugal-Spain border. The area of interest is the 100x100km² square that is equal to the size of the Sentinel-2 tile.



Figure 1: Study Area

2.1.2 Climate and Vegetation

The place is situated in the subtropical climate zone, which signifies that it is prone to forest fires. The climate is classified as a Hot-Summer Mediterranean climate. It is characterized by hot dry summers and mild winters.

The Mediterranean climate zone is associated with typical Mediterranean forests, woodlands, and shrub biomes. Extremely characteristic of this climate are sclerophyll shrublands, which typically consist of densely growing evergreen shrubs. [10]

2.2 Data

As a part of the project, for which the aim is to work with open-source data as much as possible, only open - source data was used.

The first open-source data to be mentioned are data required from CORINE Land Cover. This inventory consists of vector data and provides information on the land cover in most of Europe. The purpose of using these layers in this study was to find suitable areas for the analysis, to compare the burnt areas depicted in the CORINE Land Cover with the ones classified from the Sentinel-2 imagery.

Other crucial data were satellite multi-spectral image data, particularly data acquired from Sentinel-2 satellites (2A and 2B), which can be downloaded from the European Space Agency website using the Copernicus Open Access Hub.

2.2.1 Raster Data: Sentinel-2

Sentinel-2 satellites provide data and imagery that are central to the European Commission's Copernicus program. The project came to existence for a purpose of global observation of the Earth in a high resolution.

Each of the two Sentinel-2 (2A and 2B) satellites uses a wide-swath high-resolution multispectral imager with 13 spectral bands with a spatial resolution of 10-m, 20-m, and 60-m. Swath width is 290-km, therefore the mission is providing global coverage of the surface every 10 days (with the first spacecraft), every 5 days if both are in orbit.

These two satellites are on the same orbit (786 km above the Earth), 180° apart for optimal coverage and data delivery. The coverage limits are from between latitudes 56° south and 84° north. Both are operated by a Flight Control Team from ESOC, which is a part of the European Space Agency. Sentinel-2A has been in orbit since 23rd June 2015, Sentinel-2B since 7th March 2017. The estimated lifetime period is about 7 years. [11]

Product Types

Sentinel-2 MSI products are divided into 5 levels (product types), but only 2 of them are available for users.

The Level-0 products are compressed raw image data in IPS format. It is used as the foundation of Level-1 products.

The Level-1A products are obtained by decompressing the Level-0 data. In this product, a geometric model is developed.

The Level-1B products provide radiometrically corrected imagery in Top of Atmosphere radiance values and in sensor geometry. These products include the geometric model that is used to generate the Level-1C product.

All of these products are 25 km across track by 23 km along track granule. They are not released to users.

The first products that are available for users are the Level-1C products. They are composed of 100x100km² tiles in the UTM/WGS84 projection. These products result from using a DEM to project the image in cartographic geometry. Level-1C are resampled at 10, 20, and 60 meters. Level-1C products include Cloud Masks.

Unlike the Level-1C products, Level-2A products contain atmospheric corrections. The Level-2A product provides Bottom of Atmosphere reflectance images acquired from Level-1C products. It is also composed of 100x100 km² tiles in the UTM/WGS84 projection. These products were generated since March 2018 over Europe.[12]

Spectral Bands

The main sensor is an optical sensor MSI, a *push broom scanner* measuring the Earth's reflected radiance in 13 spectral bands. The scanner provides a wide spectral coverage over the visible, near infrared and short-wave infrared domains, with medium spatial resolution from 10-m to 60-m depending on the wavelength.

Thanks to the high revisit time of the mission, the 10-m and 20-m spatial resolution bands of Sentinel-2 A and B missions support disaster relief efforts. It includes identifying areas being at risk from natural hazards such as areas liable to burns, floods and earthquakes.

As said, MSI consists of 13 spectral bands. Four spectral bands with 10-m resolution in visible and NIR wavelengths, six spectral bands with 20-m in red edge, NIR and SWIR wavelengths and three 60-m bands for detection of aerosols, water vapor, cirrus clouds and for atmospheric correction. [13]

Spatial Resolution (m)	Band Number	S2A		S2B	
		Central Wavelength (nm)	Bandwidth (nm)	Central Wavelength (nm)	Bandwidth (nm)
10	2	492.4	66	492.1	66
	3	559.8	36	559.0	36
	4	664.6	31	664.9	31
	8	832.8	106	832.9	106
20	5	704.1	15	703.8	16
	6	740.5	15	739.1	15
	7	782.8	20	779.7	20
	8a	864.7	21	864.0	22
	11	1613.7	91	1610.4	94
	12	2202.4	175	2185.7	185
60	1	442.7	21	442.2	21
	9	945.1	20	943.2	21
	10	1373.5	31	1376.9	30

Figure 2: Wavelengths and Bandwidths of the 3 Spatial Resolutions of the MSI instruments [14]

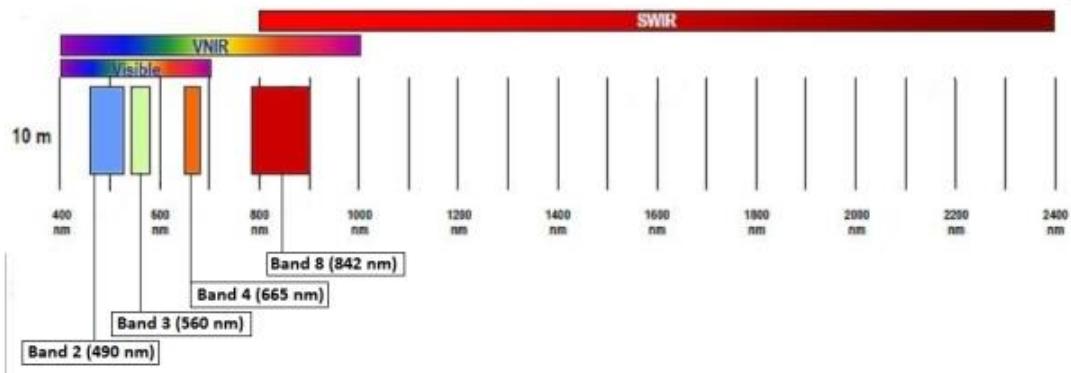


Figure 3: Sentinel-2 10 m spatial resolution bands: B2 (490 nm), B3 (560 nm), B4 (665 nm) and B8 (842 nm) [13]

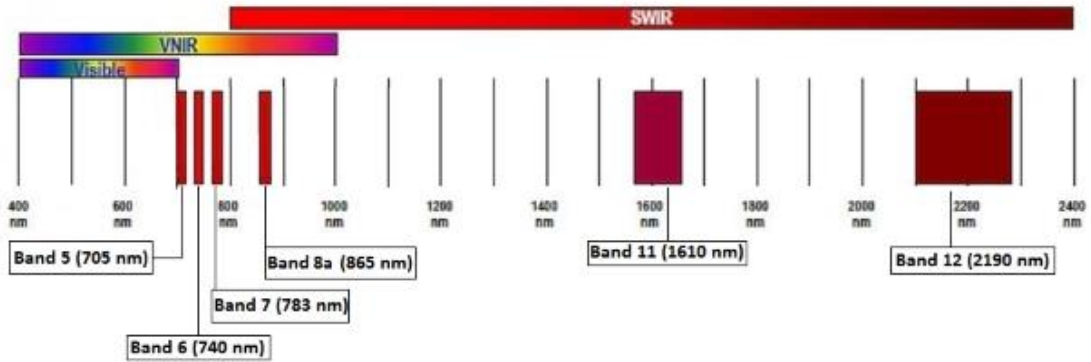


Figure 4: SENTINEL-2 20 m spatial resolution bands: B5 (705 nm), B6 (740 nm), B7 (783 nm), B8a (865 nm), B11 (1610 nm) and B12 (2190 nm) [13]

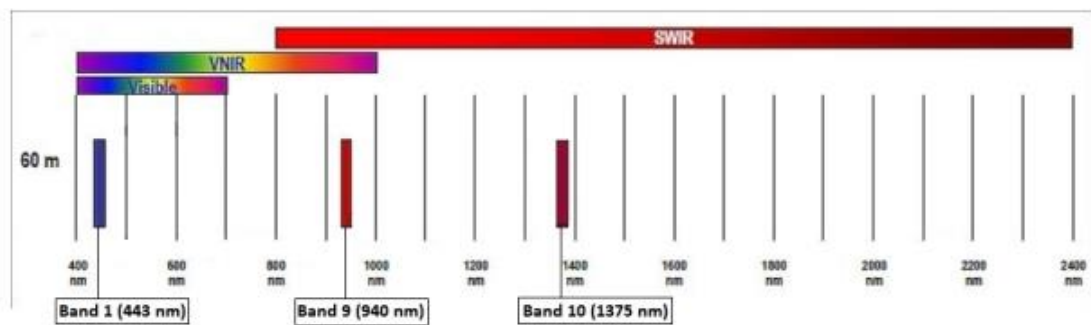


Figure 5:SENTINEL-2 60 m spatial resolution bands: B1 (443 nm), B9 (940 nm) and B10 (1375 nm) [13]

Imagery used

For the purpose of this thesis, it was needed to choose a suitable area of the frequent occurrence of forest fires. If available, summer and spring imagery was acquired (choosing of this area is described in the chapter of “Area selection”). Because of the inaccessibility of Level-2A products from every year, some of the applied images were Level-1C, which required atmospheric correction.

Eleven high-resolution, cloudless (less than 2%) images displaying the same area were captured, one from November 2015, two from 2016 (August and April), two from 2017 (beginning of September and March), two from 2018 (August and May), two from 2019 (beginning of September and the end of May), and last but not least, two images from 2020 (August and March). Each summer and spring image is chosen to have a close acquisition date to the date of fire and for the elimination of significant phenological changes.

An RGB (B4, B3, B2) natural-color image of the area of interest is displayed below in Fig 6.

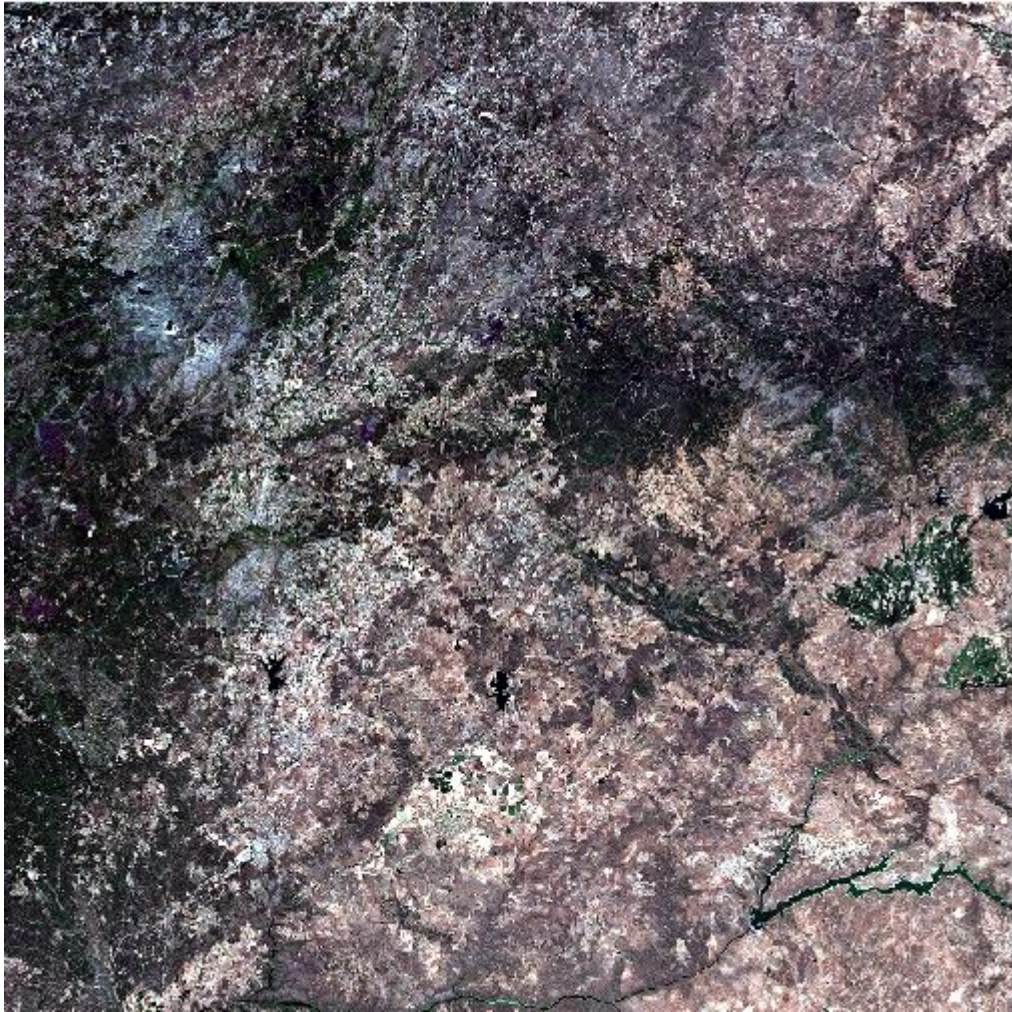


Figure 6: Sentinel-2A image of the area of interest acquired in August 2020

Tile	Acquisition Date	Sensor	Level of Product
T29TPE	2015-11-12	Sentinel-2A	MSIL1C
	2016-04-30	Sentinel-2A	MSIL1C
	2016-08-28	Sentinel-2A	MSIL1C
	2017-03-16	Sentinel-2A	MSIL1C
	2017-09-02	Sentinel-2A	MSIL2A
	2018-05-15	Sentinel-2B	MSIL2A
	2018-08-28	Sentinel-2A	MSIL1C
	2019-05-25	Sentinel-2A	MSIL2A
	2019-09-12	Sentinel-2A	MSIL2A
	2020-03-10	Sentinel-2A	MSIL2A
2020-08-27	Sentinel-2A	MSIL2A	

Table 1: Specifications of images used in this study

The following spectral bands of 10-m and 20-m spectral resolution were applied – B2, B3, B4, B5, B6, B7, B8, B8a, B11, and B12. Moreover the spectral indices are computed from a few of them. All of the 20-m resolution bands were resampled to 10-m for the following analysis.

Products

As said, input data for the workflow were the Level 1C and Level 2A products, from which indices and classification were carried out. The data preparation of both Level-1C and Level-2A products for future analysis is described.

Level-1C Product

First, in the case of Level-1C products, it is necessary to apply a TOA correction. This is done to be able to separate the actual reflectance that was given off from the object on the Earth’s surface from the atmospheric disturbances that are part of the reflected energy recorded by the sensor. [15]

The TOA correction was applied on each band in SCP in the *Preprocessing* menu. After all of the bands to be used for the following classification (all except B1, B9,

B10) were loaded, the *Apply DOS1 atmospheric correction* function was selected in the window.

After that, all of the corrected bands were resampled to 10 m spatial resolution. The resampling was performed in QGIS by SAGA's *Resampling* function. A *Nearest Neighbor* downscaling algorithm was used. This method assigns the digital number of the closest input pixel to the corresponding output pixel and it preserves original values in the unchanged scene.

Level-2A Product

Since the Level-2A product includes the atmospheric correction, only the resampling of the bands was executed. The resampling method used was the same as in the case of the Level-1C products.

Selecting the Seasons and Years

Since the satellite data which were chosen for the evaluation are available from June 2015, the period of examination lasted from 2015 to 2020. From each year, a satellite image from both spring and the end of the summer were acquired. These two seasons were chosen based on the spectral signatures of the vegetation in these times of the year and due to the forest occurrence.

Choosing the Signature Space

Another important part was a selection of the signature space. The space was based on suitable vegetation indices for detection of the burnt areas.

Regarding the initial findings from references, numerous vegetation indices¹ (new channels calculated from equation (1)-(X)) were applied to detect the forest fire and the future development of the burnt area in Mediterranean types of forest vegetation.

For our purpose, the most suitable should be vegetation indices ARVI and NDVI as well as the index NBR and dNBR. Normalized Difference Vegetation Index and Normalized Burn Ratio both play an important part in every study and indicate very

¹ combinations of surface reflectance at two or more wavelengths computed to highlight a particular property of vegetation

precise results in the case of post-fire temporal development. Due to this fact, these two indices were used in the workflow of this thesis.

The use of dNBR also seemed to be very helpful according to the research (*Lasaponara, Tucci and Ghermandi, 2018*). Based on the research, dNBR, calculated from the NBR pre and post-fire, was used to estimate the burn severity. A higher value of this differenced index shows more serious damage, whereas the negative dNBR values indicate regrowth following a fire. From the dNBR, burn severity levels can be obtained.

Another index that was used in the study is an Atmosphere Resistant Vegetation Index. According to the first study mentioned here (*Barbosa, Caetano and Santos, 2000*), the index indicated high values for vegetation cover, low values for forest burnt areas, and even lower values for terrain mobilization.

Modified Soil Adjusted Vegetation Index is not suitable for the examination. As said, since the correlation between MSAVI and vegetation cover is high, values delivered from MSAVI from imagery acquired in the dry period can be used to estimate the water storage capacity. Nevertheless, this index could be used only if the area had not been affected by fires for a long time (*Gallaun and Banninger, 1996*).

Another index mentioned is a Soil-adjusted Vegetation Index. Based on the study, post-fire SAVI spatial values showed a relatively rapid regeneration compared with NDVI. The use of SAVI to determine post-disturbance recovery could be an alternative option to NDVI (*Tonbul, Kavzoglu and Kaya, 2016*). For the purpose of this thesis, it was decided to choose NDVI rather than SAVI because this index is used more frequently for the burnt areas' analysis.

However, since this thesis aims to get more accurate results and find a different, simple way of burnt area detection and temporal development, modifications of the workflow were necessary.

Computation of indices is one of the methods of spectral image enhancement. It is used to distinguish subtle spectral changes. The resolution can be improved because the image created by dividing the two bands shows changes in the slopes of the spectral

reflectance curves between the two bands regardless of their absolute values. These changes are different for each material in some bands.

Normalized Difference Vegetation Index (NDVI)

The first vegetation index used to determine the burnt region was NDVI. This index is well known for identifying the vegetated areas and their condition.

The NDVI is computed both from NIR and R bands, which stand for the spectral reflectance measurements acquired in the red and near-infrared regions:

$$NDVI = \frac{NIR-R}{NIR+R} \quad (1)$$

For Sentinel-2, it is defined as:

$$NDVI = \frac{B8-B4}{B8+B4} \quad (2)$$

The NDVI values range from -1 to +1. The low values (-0.1 to 0.1) show the absence of vegetation (e.g. water, urban areas, rock, sand, snow, or burnt areas), the positive values represent shrub and grassland (0.2 to 0.4). If there is much more reflected radiation in NIR wavelengths than in the visible ones, the vegetation in this pixel should be dense. It means that high values (0.5 to 1) indicate dense and healthy vegetation.[16]

Atmospherically Resistant Vegetation Index (ARVI)

To reduce the dependence of the atmospheric effects, in comparison to NDVI, this modification was developed by *Kaufman and Tanré, 1992*.

The modification includes the atmospheric information contained in the blue channel:

$$ARVI = \frac{NIR-RB}{NIR+RB} \quad (3)$$

In Sentinel-2:

$$ARVI = \frac{B8-RB}{B8+RB} \quad (4)$$

Where RB is a combination of the B and R channels:

$$RB = R - \gamma(B - R) \quad (5)$$

Sentinel-2:

$$RB = B2 - \gamma(B2 - B4) \quad (6)$$

For a purpose of this study, γ (an atmospheric self-correcting factor) was set to 1 since the aerosol model is not available.

The ARVI values should show similar values to the NDVI. According to the study (*Barbosa, Caetano and Santos, 2000*), ARVI has a similar dynamic range, but it is four times less sensitive to atmospheric effects than the NDVI. [17]

Normalized Burn Ratio (NBR)

The NBR is an index used for detecting the burnt areas and classifying their severity. It was first used by *Key and Benson, 2005* for fire effects monitoring. The formula is similar to the NDVI, but the SWIR wavelength is used instead of the R wavelength:

$$NBR = \frac{NIR-SWIR}{NIR+SWIR} \quad (7)$$

In Sentinel-2 defined as:

$$NBR = \frac{B8-B12}{B8+B12} \quad (8)$$

As said, healthy vegetation shows very high reflectance in the NIR and the low reflectance SWIR. In the case of burnt areas, it is the opposite. High NBR values depict healthy vegetation, and a low value indicates bare soil or an area recently affected by the fire.

Burn severity is interpreted by the differenced NBR, which is going to be described later.

All these three indices were used for the supervised classification as additional channels to the Sentinel-2 bands B2, B3, B4, B5, B6, B7, B8, B8a, B11, and B12.

2.2.2 Vector Data: CORINE Land Cover

The Corine Land Cover inventory was initiated in 1985 by the European Commission. The first product appeared in 1990, and since the year 2000 is updated every 6th year (2000, 2006, 2012, 2018). The CLC consists of 44 land cover classes. Land cover classes are displayed below (Fig.7).



Figure 7: CLC Classes [18]

The CORINE Land Cover database is created Europe-wide on a 1 : 100 000 scale. It uses a Minimum Mapping Unit of 25-ha for areas and a minimum width of 100-m for linear phenomena. A detailed description of the CORINE data collection methodology and definition of classes are available at [19].

For the aim of this work, mainly data from CLC 2018 were used. CLC data from 2006 and 2012 serve for the primal visual comparison of the burnt area classes.

The base for the CORINE Land Cover 2018 is satellite data from Sentinel-2 and Landsat 8 for gap filling. The geometric accuracy of these satellite data (Sentinel-2) is ≤ 10 m. The geometric accuracy for CLC is better than 100 m, thematic accuracy is $\geq 85\%$. Access to the data is free for all users. [20]

Burnt Areas

Burnt Area class is defined in CLC as natural woody vegetation cover affected by recent fires. This class includes burnt areas within a year of image acquisition, burnt forest areas, sclerophyllous vegetation, moors and heathlands, transitional woodland-shrub, and areas with sparse vegetation. Burnt areas are visible on satellite images in a black, dark green, or grey color.

The class also includes damaged natural woody plants, damaged natural herbaceous plants among burnt woody plants, bare soil, and rock covered by ash.

It excludes damaged crops, however, and it is not applicable for burnt areas where: the signs of fresh burn are not visible anymore and $> 50\%$ of area is non-vegetated, burnt areas where regeneration has already started on $> 50\%$ of area, burnt natural grassland, burnt permanent crops, or human farming management by burning arable lands.[21]

2.3 Image Processing

The next part is to carry out a supervised classification of the study area. For the classification and following analysis, QGIS 3.16.3 was used.

The Maximum Likelihood classification method was used. This method of classification in the context of burnt areas analysis was mentioned in one of the studies (*Patrono, Baptista, and Ebeltes, 2000*) and seemed to be one of the best classification methods to be executed.

For the aim of the supervised classification, the training and testing areas were chosen carefully.

After the classification had been carried out, the accuracy of the training and test areas were computed to get as accurate as possible results.

2.3.1 Classification

Generally, classification is a process, during which certain informative values are assigned to the individual pixels. It aims to replace the values of the radiometric characteristics of the original image, which shows the spectral properties of objects, by values expressing *classes*. By this process, which gives information about the types of the objects and is defined by pixels with the same digital values, the map is created. The classification is based on the usage of certain decision-making rules, so called *classifiers*, according to which all elements of an image can be assigned to a certain class.

In remote sensing, the classification *pixel per pixel* is used the most frequently. Another type of classification is a *segment-based* classification (composed of more pixels). This classification method is used chiefly in the case of data in high resolution.

The classification rule must be known for executing the classification. This rule indicates a relationship that assigns the digital values of image data to the relevant parameter value (e.g. type of a land cover). By this process, the values are assigned to a specific class.

In the majority of the cases, the information classes are not directly recorded in the image data. Nevertheless, they can be found indirectly, through radiometric characteristics of individual pixels in a multispectral image. On the other hand, image data contain so-called spectral classes, which are the parts of the image that are homogeneous in terms of their spectral behavior. The class predominantly contains several spectral classes, but it depends on the specific classification scheme and the classification's focus.

The classification rules are composed by the *classification signatures*. There are many types of these signatures – spatial, spectral, temporal, or polarizing. However, in this study, only the spectral signatures were used. The rule was unknown and needed to be created.

In general, a classification can be divided into an *unsupervised* or *supervised classification* according to how and at which point the processor intervenes in the classification process. These two types of classification can also be combined.

Unsupervised classification is a method in which the software separates a large number of unknown pixels (based on their reflectance values) into clusters or classes. The processor is to find out what the individual classes represent.

2.3.2 Supervised Classification

In this study, supervised classification was used. The supervised classification provides a possibility of creating the classes prior to classification itself by the processor. Classification rule is done by the *training set*, which is created by the processor [22] [23]. The classification is based on the idea that a processor can select the sample pixels representing specific classes themselves.

To carry out the classification, it is needed to choose the right classifier. There are a lot of options for classifiers. The choice of the classifier depends on the nature of the input data and desired output. For this study, the Maximum Likelihood classification algorithm was used.

Maximum Likelihood

This statistical method assumes that the distribution of points forming one class of training data has a Gaussian distribution.

In remote sensing, a *Maximum Likelihood* classification finds out the likelihood that a given pixel belongs to a specific class. Each pixel is assigned to the class based on the highest probability (if the threshold is not defined). *Maximum Likelihood* is one of the most used types of classifier in remote sensing. [22]

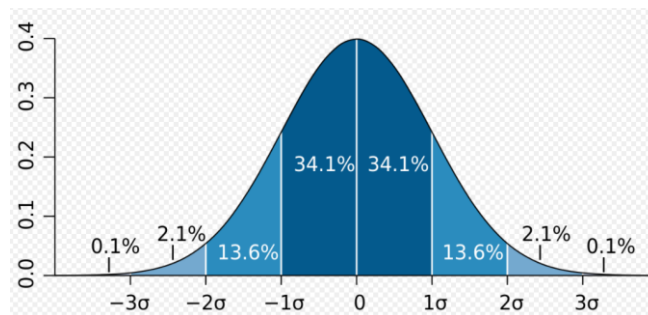


Figure 8: Gaussian distributin. Source:Wikipedia

Classification Process

The classification set of signatures is created from the training areas. To define the training areas for each class, the ROI (Region of Interest) tool was used.

Firstly, the classification was executed only using the combination of three vegetation indices – NDVI, NBR and ARVI. The result of the classification was not accurate at all, so it was needed to think up another combination of multi-band raster to be used as a ground truth for the classification.

After that, the multi-band raster was created, composed the 13 corrected and resampled bands (10 plus 3 indices). The training input *.scp* was used for storing ROIs and spectral signatures of the training areas.

After the definition of classes, the classification was carried out. The SCP enables using three types of classifiers – *Minimum Distance*, *Maximum Likelihood*, and *Spectral Angle Mapping*. The first classifier was not even tested. The reason is that in these types of classifiers, the objects that are classified are groups of measurement vectors – all of them are in one field, rather than individual vectors. The results of the classification computed from both the *Spectral Angle Mapping* and *Maximum*

Likelihood were compared (only visually) to each other. The *Maximum Likelihood* method was chosen based on the visual comparison.

After carrying out the classification, the “salt and pepper” pixels, which occurred in the classified image, were eliminated by the *Sieve* function available in QGIS. This function removes smaller polygons than a provided threshold size and replaces them with the pixel value of the largest neighbor polygon. [24] The threshold for eliminating the pixels was selected based on the classification results of each scene. The minimum was 10 pixels and the maximum 30 pixels.

All eleven scenes were classified the same way. The accuracy and the results of the classification are described in the following chapters.

Training set

Selection of the training set is one of the most crucial parts of supervised classification. The training areas must be selected carefully, based on the processor’s knowledge of the area of interest. The number of samples for each class should be selected according to the object’s occurrence and samples should be positioned throughout the image. The number of training areas depends on the number of categories to be mapped or their diversity.

Firstly, for the whole classification process, the legend and training areas needed to be defined. The legend itself followed from the literary sources dealing with the analysis of the burnt areas, and field research of the area of interest.

Five classes based on their spectral signatures were defined. Even though the area of interest is heterogeneous, it emerged that for the detection of the areas affected by fire, it was enough.

The training areas were selected primarily according to the spectral signatures in the NDVI, computed from the NIR and R bands from Sentinel-2, and the aerial photograph of the area in real colors. The input image was displayed in RGB ($R = SWIR$, $G = NIR$, $B = R$). This combination of bands allowed better visibility of the condition and density of the land cover, including the burnt areas. The training areas were selected based on their occurrence and size of the objects.

The classes selected for the classification were following:

1 Burnt Areas

2 Water

3 Non – Vegetated Areas

4 Sparse Vegetation

5 Dense and Green Vegetation

These classes were defined for all eleven scenes, which were used as a ground truth for the classification. The reference data composed of all 10 bands (B2, B3, B4, B5, B6, B7, B8, B8a, B11, B12) plus the vegetation indices (NDVI, ARVI, NBR) for better results.

The most important and the most difficult issue while creating classes was the selection of the areas for the “Burnt Areas” class. This was done by visual observation of the area of interest in the infrared color combination of spectral bands through the *Sentinel Hub Playground*. The combination of sentinel bands B8, B4, and B3 enables us to see the locations affected by fires very clearly. These areas are distinguishable because of their back, dark grey or light grey color. The color depends on the age of the burnt area.



Figure 9: Burnt area (based on Sentinel-2 bands B8, B4, B3). Source: Sentinel Hub Playground

After the selection of the training areas and their assignment to the classes, their separability was checked by *histogram* and *scatter plot*. A histogram showed that training areas corresponded to several different object classes at once. The spectral separability was also checked by the scatter plot, which demonstrated almost no overlap of the classes. However, it was observed that the “Burnt Areas” class may be confused with the “No Vegetation” class. Despite this fact, the classification was performed.

Selection of the Test Areas

For an objective accuracy assessment, it is necessary to use reference data that are not the same as training sets. This data serves for the processing of the contingency table. The test areas are usually represented by either homogeneous test areas preselected by the processor or randomly selected pixels. The second option usually gives a bad picture of the classification result, because the number of the selected pixels is commonly very low. That’s why the first option was selected for our purpose.

The representative homogenous test areas differ from the training areas and are considerably larger. The training and test areas were selected identically and the number of the test areas for each class was lower than training areas.

Accuracy Assessment

The last step of the classification is the accuracy assessment. In this study, the assessment was done using a classification error matrix (also called confusion or contingency table). It is one of the most common means of expressing classification accuracy. This matrix works on a category-by-category basis, where the input (reference) data are compared to the corresponding test data. It shows how the pixels from the training set are assigned to each of the classes. If the number of pixels of training areas assigned to a different class (values off the diagonal of the error matrix) is high, it indicates that the training areas are not selected appropriately – the classes overlap. In this case, it is necessary to select a more suitable training set and repeat the classification. The diagonal cells of the matrix contain the number of correctly identified pixels.

Another possible way to check the accuracy of the training areas is to use a scatter plot. It is a graph, in which the values of selected areas of each class from one band are plotted (one band on one axis). If the separability of the classes is fine, then the clusters of pixel values in training areas don't overlap.

The next part of the assessment is an evaluation of accuracy by creating test areas. These samples are not identical to the training ones.

The accuracy can be assessed by several methods:

- 1) **Overall Accuracy** – this accuracy is computed by dividing the sum of the correctly identified pixels by the total number of pixels

$$OA = \frac{1}{n} \sum_{k=1}^N a_{kk} \quad (9)$$

where

n = total number of pixels used for training or test areas

N = total number of classified classes

a_{kk} = correctly identified pixels

- 2) **Average Accuracy** – this averages the number of correctly classified pixels of each class

$$AA = \frac{1}{N} \sum_{k=1}^N a_{kk} \quad (10)$$

- 3) **User's Accuracy** – defines the number of correctly identified pixels of a class, divided by total number of pixels of the class in the classified image

$$UA_i = \frac{a_{ii}}{\sum_{k=1}^N a_{ik}} \quad (11)$$

where

$\sum_{k=1}^N a_{ik}$ = total number of pixels classified to the given class

- 4) **Kappa Index** – a measure of how the classification results compare to values assigned by chance

$$\kappa = \frac{P_0 - P_C}{1 - P_C} \quad (12)$$

where

P_0 = agreement between reference data and classified image

P_C = agreement by chance

The range of the kappa coefficient is from 0 to 1. The higher kappa index, the more accurate classification. If the kappa index equals 1, the classification is faultless.[22]

The selection of the training and test data in this thesis is explained in the following chapters.

2.4 Temporal Development

Classified burnt areas were compared with the burnt area class determined from CORINE Land Cover. As mentioned, it was determined, whether the burnt areas were visible in the CLC burnt area class or not, and if so, in what type of vegetation appeared and for how long the burnt areas classified from the Sentinel-2 images could be distinguished in CLC.

The next step was to show the temporal analysis of the burnt areas in the different types of forested areas. It was done by computation of the mean values, standard deviation, modal values, and median of each area and their evolution in time. This development was displayed in graphs and additional tables.

2.4.1 Selection of Burnt Areas

At first, it was necessary to select the “Burnt Areas” class from the classified image for the following analysis. It was carried out using the Raster Calculator tool in QGIS. After the “Burnt Areas” class selecting, a new raster layer was created - containing values 1 (for burnt areas) and 0 for the rest of the analyzed scene. This raster had to be converted to a vector layer to perform analysis of the concordances and differences between the classified burnt areas and CLC Burnt Areas class. The raster was converted using the *Raster to Vector* function in QGIS.

Since the CLC and scenes from Sentinel-2 have a different reference coordinate system (CLC-ETRS89 and Sentinel-2-WGS84), the CLC Burn Area class was converted to WGS84 to prevent potential errors. This was executed using the *Reproject Layer* function

2.4.2 Comparison

Firstly, the visual comparison was executed. It was necessary to find out when the burnt area occurred for the first time (before or after the acquisition at a specific scene) to calculate the approximate time when the fire broke out.

Every two consecutive scenes were visually compared to each other to find out the concordances and differences. It was done using *Sentinel Hub Playground*. According to the information required, most of the fires broke out in summer, which was predictable because of the type of climate and its behavior during the year – dry and warm summer and rainy fall/winter. There were only two exceptions - years 2017 and 2018, in which forest fires occurred in late September – the burnt areas from this period are recognizable from the spring scene from the following year for the first time.

The next issue to be solved was to determine for how long it was possible to detect the burnt areas and whether they were mapped in CORINE Land Cover.

Comparison with CLC

At first, classified burnt areas from November 2015 were compared to the Burnt Area classes from CLC 2012 and 2018. It was carried out through the *Intersection* function in QGIS.

In CLC 2012, there was no identical burnt area in comparison with the classified scene from 2015. In the case of the year 2018, three places were registered in CLC as well as in the 2015 classified scene.

Other classified burnt areas from remaining years (2016, 2017, 2018) were only compared to CLC 2018.

There were no new classified burnt areas from the April 2016 scene and one identical burnt area to CLC 2018 in the case of September 2016.

The classified scene from March 2017 had also no identical burnt areas to the CLC 2018. However, in the classified scene from September 2017, six identical areas to the CLC 2018 were found.

The burnt areas classified in the scenes from 2018 are not registered in CLC 2018 at all.

The classified areas registered in CLC 2018 (Table 2):

SCENE	AREAS - TYPE OF VEGETATION
November 2015	Area 1 – Sclerophyllous vegetation
	Area 2 – Moors and Heathlands
	Area 3 – Moors and Heathlands
September 2016	Area 1 – Transitional woodland-shrub
September 2017	Area 1 – Transitional woodland-shrub + Moors and Heathlands
	Area 2 – Transitional woodland-shrub + Moors and Heathlands Transitional woodland-shrub
	Area 3 - Moors and Heathlands
	Area 4 - Transitional woodland-shrub + Coniferous Forests
	Area 5 – Transitional woodland-shrub
	Area 6 - Coniferous Forests

Table 2: Classified burnt areas registered in CORINE Land Cover 2018

Comparison with classified Burnt Areas

The classified areas from each summer (or fall in the case of the year 2015) were compared to other classified burnt areas from every remaining year (both spring and summer).

Firstly, the classified areas from each year were divided into several groups depending on their detectability in the following years. For example, for the year of 2015, **five groups** were defined – detectable after 1st year (2016), 2nd year (2017), 3rd year (2018), 4th year (2019), and 5th year (2020).

In each group, the burnt areas were divided into **two other groups** – identical areas classified in a specific year following the first detection or identical areas not classified in the same year (in the case of 2015, there were 10 groups). It enabled the recognition of the length of the detectability of the burnt areas. It was determined whether the burnt areas were recognizable from both scenes in a specific year following the fire or only from one of them.

It was performed using the *Raster Calculator* function. As said, value 1 was assigned to the burnt areas and value 0 to the rest. To find out the common burnt areas, a new raster containing values 0 and 1 was computed using this command: (“1st raster” = 1) & (“2nd raster” = 1). This new raster showed the common burnt areas. To find out the burnt areas that are distinguishable in the first scene and not in the other one, the

command (“1st raster” = 1) & (“2nd raster” = 0) was used. Another raster containing values 0 and 1 was computed. This process was carried out for each pair of scenes (both spring and summer from each year). The scheme of the process is shown below (Fig.10):

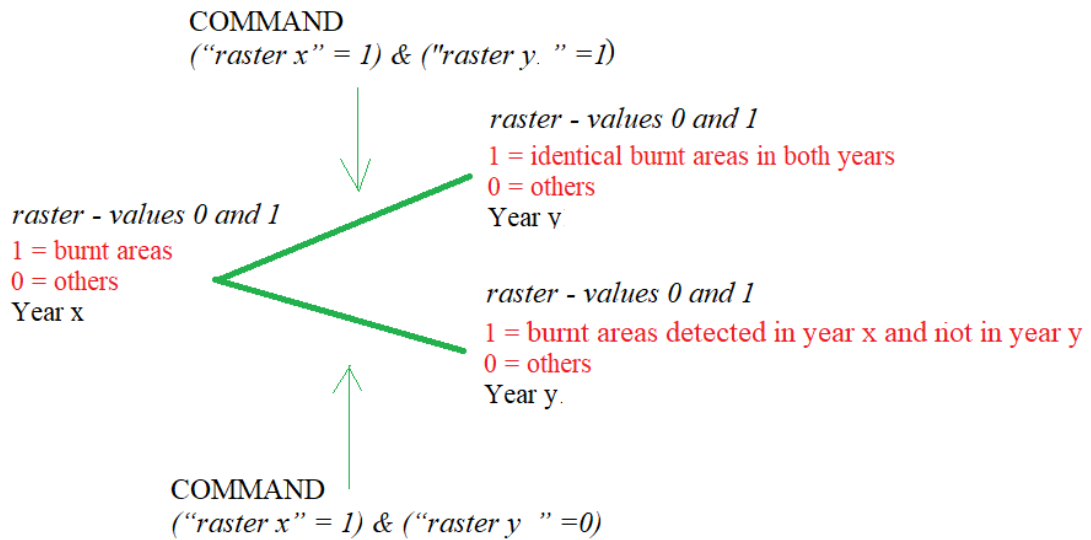


Figure 10: Scheme of the burnt areas' comparison

2.4.2 Selection of the Areas to be analyzed

For the temporal development analysis, it was necessary to select the areas of examination. The layers (for each type of forest and depending on the period of the first burnt area's detection) were created and used for the following computation of the statistics. This selection of the areas and their assignment to the layers were the first steps for the temporal analysis. These were used for the temporal analysis using the values computed from the *Zonal Statistics*. In this chapter, the selection of the areas is delineated.

Division of the Burnt Areas

The analysis described above helped to determine the detectability of the burnt areas in the following years after each fire. According to the analysis, the longest detection period was approximately three years since the fire broke out. The temporal development and regeneration of the burnt areas might depend on the type of the

forested area. That's why the sorting of all detected burnt areas, based on the vegetation type of forest, was needed.

The types of the forested areas affected by fire are the following:

- TRANSITIONAL WOODLAND-SHRUB
- CONIFEROUS FORESTS
- MIXED FORESTS
- SCLEROPHYLLOUS VEGETATION

The temporal analysis of the burnt areas, caused by the fire events in these types of forests, was executed. Other burnt areas that occurred in different types of land cover did not take part in the analysis. The reason is the definition of the CLC Burnt Areas class (described in chapter 4.1.1). However, this class contains the *moors and heathlands*, which were not part of the temporal development analysis because it was not possible to find out reliably if the original land cover was *moors and heathlands* (this was not recognizable from the aerial photographs or from true color images).

The division was carried out based on the true color image (or aerial photograph) and CLC. The initial selection was done by checking the CLC 2012 representation of classes in the later affected area. This was used to determine the approximate type of land cover. After that, the true color image was checked to make sure that it was the type of forest that is represented in CLC.

Four new vector layers (*Transitional Woodland-shrub*, *Coniferous Forests*, *Mixed Forests* and *Sclerophyllous Vegetation*) were created from the vector layers of burnt areas acquired from the classification output. These layers contained all the burnt areas classified from every scene (every year). The number of burnt areas in each forested area in total is shown in Table 3:

Layer	NUMBER OF BURNT AREAS
<i>Transitional Woodland-shrub</i>	11
<i>Coniferous Forests</i>	1
<i>Mixed Forests</i>	2
<i>Sclerophyllous Vegetation</i>	1

Table 3: Number of Burnt Areas in each layer

Selection of the Forested Areas untouched by fires

For performing the temporal analysis, it was necessary to compare the temporal development of the burnt areas with the development of the areas not affected by the fire. As in the previous case, the areas were divided into classes saved in four layers (*Transitional woodland-shrub*, *Coniferous forests*, *Mixed forests*, and *Sclerophyllous vegetation*). These layers represented homogenous areas for each group. The selected forested areas had approximately the same size as the burnt areas representing them and were selected to be in the vicinity of the burnt areas. The number of forested areas was identical to the number of burnt areas in each vegetation group.

2.4.3 Computation of dNBR

At the beginning of the study, it was decided to use the dNBR index as well as the other vegetation indices (NDVI, ARVI, NBR) for the temporal development analysis. The computation of this index is mentioned in this section because dNBR was not a part of the previous classification.

The computation of dNBR is quite different from the computation of other indices. It is created with the aid of pre-fire and post-fire NBR images. This index is used to estimate the burn severity. While differencing (*prefire* – *postfire*), a more positive value indicates more severe damage, the more negative (regrowth). [25] The formula is defined as:

$$dNBR = prefireNBR - postfireNBR \quad (13)$$

In the terms of this thesis, the dNBR was computed not only for pre and post-fire images; it was computed for every two consecutive scenes to be able to show (primarily in graphs) the gradual development of the values of dNBR in each given period.

2.4.4 Statistical Evaluation

The statistical analysis shows the development in a table and graphical forms. The **mean, modal, median value** and **standard deviation** were computed and then depicted in graphs. Additionally, the maximum and minimum value for each area was calculated.

At first, it was necessary to clip acquired NDVI, ARVI, NBR, and dNBR images for each period, by the extent of each of all 30 selected areas. It was carried out using *r.mask.vect* tool that was available in QGIS with GRASS. The input for this tool was a vector layer (burnt / forested area) and a raster one (for index values). The reason why the process was executed for every period, not only for the ones post-fire, was that the temporal development of the specific areas before the fire was important for the comparison of the whole development. The values mentioned in the first paragraph determined the radical changes in values that followed the fire.

The values were obtained using the *Zonal Statistics* tool. All of the results for each type of forest – mean, median, mode, standard deviation, minimum and maximum value – are attached to the thesis in the tables (*Attachment 1, Attachment 2, Attachment 3, Attachment 4*). The created graphs are displayed and described in the chapter 3.2.

2.5 Software

2.5.1 QGIS

QGIS is a multiplatform open-source geographic information system, which gives the ability to capture and analyze spatial and geographic data. It has a wide community of users and provides various types of plugins. Being developed as open-source, it renders long-term sustainability of the functioning of the workflow.

This project was founded in 2002 and its first version came out in 2009. It was originally called Quantum QGIS, however in 2013 it was renamed QGIS.

QGIS contains a lot of tools including the GDAL library, GRASS tools, and SAGA tools. One of the important qualities of QGIS is the possibility to install a wide number of plugins. Two of these are used in the study – the GRASS Plugin and the SCP Plugin (both described in the chapters below).

For the aim of this thesis, the QGIS 3.16.3 Hannover is being used.[26]



Figure 11: QGIS logo [26]

Semi-Automatic Classification Plugin

This plugin allows supervised classification and its pre and post-processing analysis. A supervised classification can be applied to remote sensing images.

It was developed by Luca Congedo. SCP can be applied on satellite images – the downloading of data from ASTER, GOES, Landsat, MODIS, Sentinel-1, Sentinel-2, and Sentinel-3 is available, as well as many algorithms of classification. The plugin requires the installation of GDAL, Numpy, OGR, SciPy, and Matplotlib. [27]

2.5.2 GRASS

The Geographic Resources Analysis Support System (GRASS) GIS is a multiplatform open-source GIS, which is used as a tool for analysis of 2D/3D raster and vector data, image data and provides a high-quality graphic output.

GRASS was first released in 1982. In the beginning, it was being developed by Construction Engineering Research Laboratory for environmental research. After that, numerous private companies, US federal agencies, and universities joined.

Since 1997, developers from around the World have been continuing in the development and release. [28]



Figure 12: GRASS GIS logo [28]

QGIS with GRASS

This plugin provides the use of GRASS tools and databases. It includes analysis of raster and vector layers, their digitalization, editing attributes, and analyzing vector and raster layers with more than 400 GRASS modules. [29]

3 Results

3.1 Classification Results

In this part, the overall results of the classification are shown. The visual interpretation of all classified scenes and the accuracy assessment are depicted below.

- 1 - Burnt Areas
- 2 - Water
- 3 - Non-vegetated Areas
- 4 - Sparse Vegetation
- 5 - Dense and Green Vegetation

Figure 13: Legend

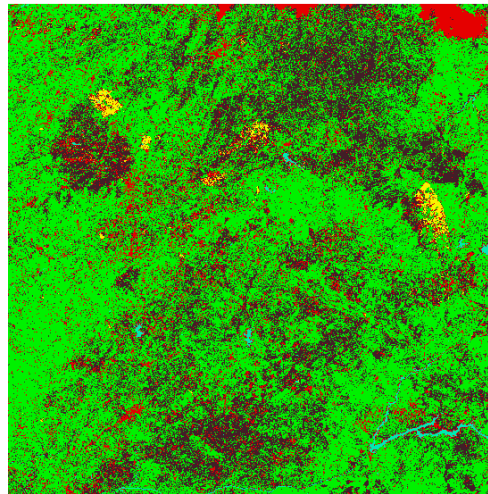


Figure 14: Classified scene from November 2015

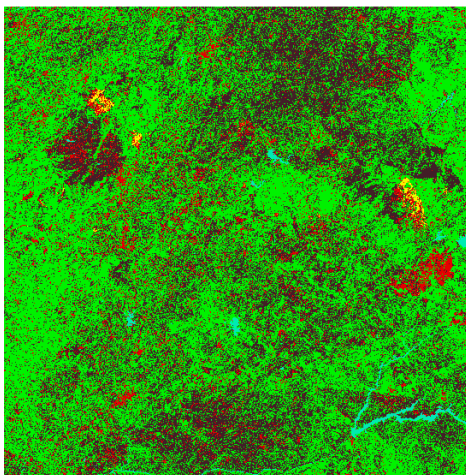


Figure 15: Classified scene from April 2016

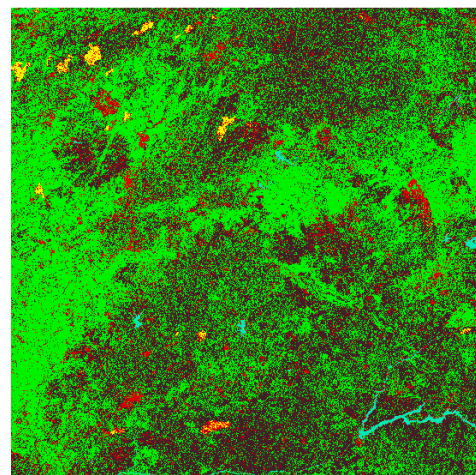


Figure 16: Classified scene from August 2016

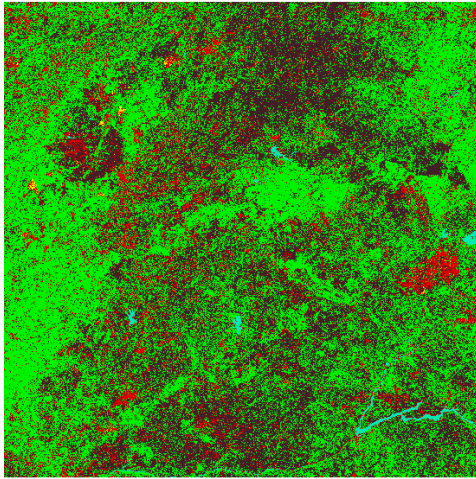


Figure 17: Classified scene from March 2017

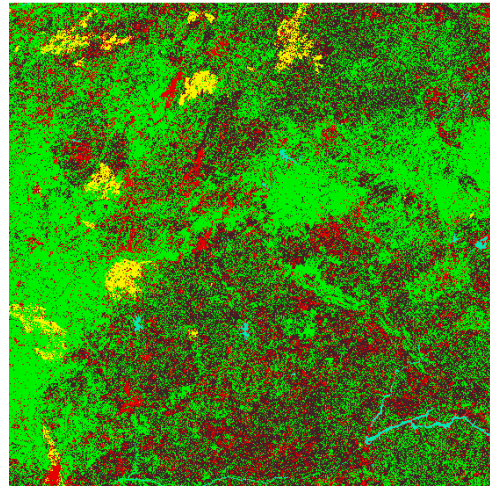


Figure 18: Classified scene from September 2017

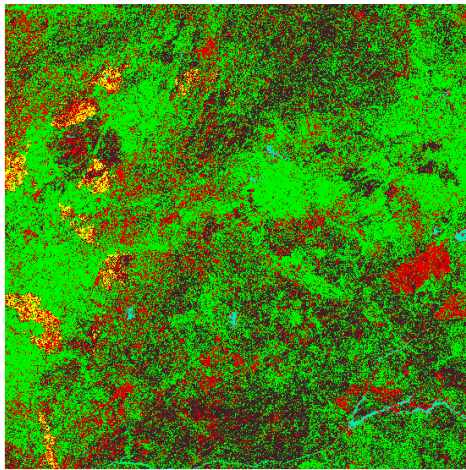


Figure 19: Classified scene from May 2018

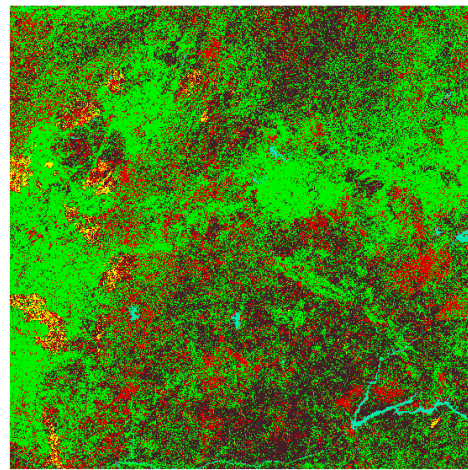


Figure 20: Classified scene from August 2018

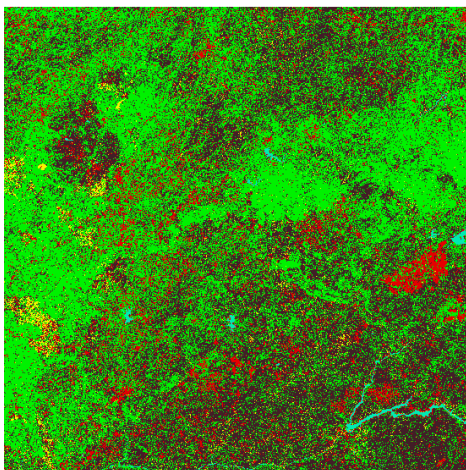


Figure 21: Classified scene from May 2019

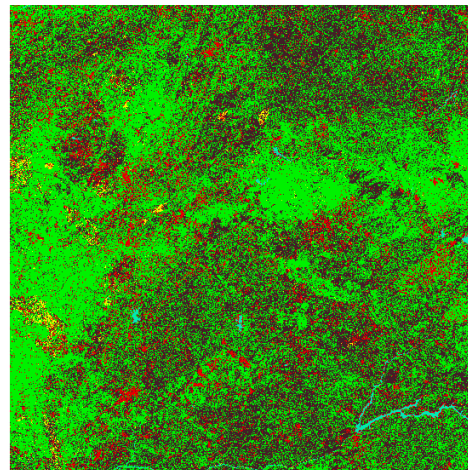


Figure 22: Classified scene from September 2019

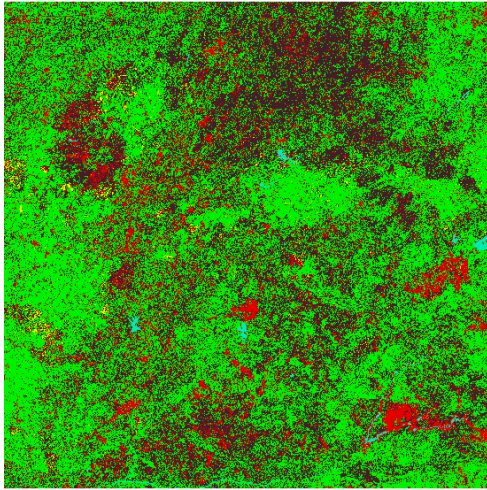


Figure 23: Classified scene from March 2020

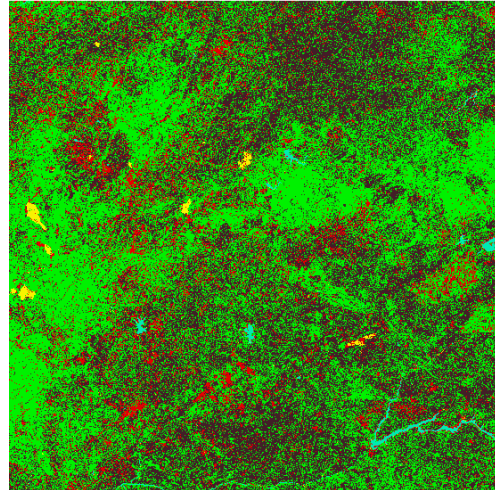


Figure 24: Classified scene from August 2020

From the classification output, it is obvious that the greatest number of fires occurred during summer 2017 (Fig.18). Also, at first glance, the temporal development of burnt areas from 2017 is recognizable. A few burnt areas continued to appear until March 2020.

Other significant burnt areas are visible in the classified image from May 2018 (Fig.19). It was calculated that the fires occurred in September 2017, which is why these burnt areas are not distinguishable in the scene from August 2017.

From this, it can be deduced that it is possible to classify the burnt areas three years after the fire started. The next chapters deal with the temporal development of the burnt areas in detail.

The following tables depict the accuracy assessment of the classification. The number of correctly and wrongly assigned pixels, and sum of pixels. The assessment was realized using the confusion matrix by which the Overall Accuracy (OA) and Kappa Index were computed.

The accuracy was performed in SCP, using the post-processing tool *Accuracy*. All of the values in confusion matrix are represented in pixels. As well as the training sets, the testing areas were selected based on the visual interpretation of the land cover in Sentinel-2 data and aerial photographs.

According to the accuracy results (Table 4, 5, 6, 7), the greatest confusion is between classes “Sparse Vegetation” (Class 4) and “Dense Vegetation” (Class 5).

CLASS	1	2	3	4	5	TOTAL
1	3266	2	4	0	0	3272
2	1	1726	0	0	0	1727
3	369	84	3245	25	69	3792
4	0	0	192	3988	95	4275
5	0	0	0	368	7100	7468
TOTAL	3636	1812	3441	4381	7264	20534

Table 4: Confusion Matrix (November 2015)

OA [%]	93.6400
Kappa	0.8859

CLASS	1	2	3	4	5	TOTAL
1	851	0	1	0	0	852
2	0	1756	0	0	0	1756
3	16	56	3188	87	48	3395
4	0	0	142	3711	1039	4892
5	0	0	110	583	6177	6870
TOTAL	867	1812	3441	4381	7264	17765

Table 5: Confusion Matrix (April 2016)

OA [%]	85.4630
Kappa	0.7407

CLASS	1	2	3	4	5	TOTAL
1	2504	3	0	0	0	2507
2	0	1534	0	0	0	1534
3	37	172	3348	145	28	3730
4	0	0	39	3580	773	4392
5	0	103	54	656	6463	7276
TOTAL	2541	1812	3441	4381	7264	19439

Table 6: Confusion Matrix (August 2016)

OA [%]	90.7900
Kappa	0.8583

CLASS	1	2	3	4	5	TOTAL
1	1288	0	47	0	0	1335
2	0	1700	0	0	0	1700
3	10	112	3252	140	50	3564
4	4	0	56	3762	456	4278
5	0	0	86	479	6758	7323
TOTAL	1302	1812	3441	4381	7264	18200

Table 7: Confusion Matrix (March 2017)

OA [%]	91.3052
Kappa	0.8839

The biggest confusion (Table 8, 9, 10). is between classes “Sparse Vegetation” (Class 4) and “Dense Vegetation” (Class 5).

CLASS	1	2	3	4	5	TOTAL
1	12683	8	0	0	0	12691
2	0	1759	0	0	0	1759
3	6	14	2994	235	83	3332
4	34	0	377	3677	668	4756
5	9	31	70	469	6513	7092
TOTAL	12732	1812	3441	4381	7264	29630

Table 8: Confusion Matrix (September 2017)

OA [%]	93.2408
Kappa	0.8991

CLASS	1	2	3	4	5	TOTAL
1	3922	3	23	23	0	3971
2	0	1555	0	0	0	1555
3	154	216	3170	347	11	3898
4	9	0	224	3576	429	4238
5	13	38	24	435	6824	7334
TOTAL	4098	1812	3441	4381	7264	20996

Table 9: Confusion Matrix (May 2018)

OA [%]	90.3904
Kappa	0.7860

CLASS	1	2	3	4	5	TOTAL
1	2769	1	27	5	0	2802
2	0	1796	0	0	0	1796
3	61	8	2969	242	19	3299
4	19	0	234	4068	853	5174
5	1	7	211	66	6392	6677
TOTAL	2850	1812	3441	4381	7264	19748

Table 10: Confusion Matrix (August 2018)

OA [%]	90.5532
Kappa	0.7812

The largest confusion in the classified scene from May 2019 is between “Sparse Vegetation” (*Class 4*) and “Dense Vegetation” (*Class 5*) classes (Table 11).

CLASS	1	2	3	4	5	TOTAL
1	2143	1	95	9	21	2269
2	0	1787	0	0	0	1787
3	4	0	2919	63	33	3019
4	27	0	426	4256	333	5042
5	2	24	1	53	6877	6957
TOTAL	2176	1812	3441	4381	7264	19074

Table 11: Confusion Matrix (May 2019)

OA [%]	88.3548
Kappa	0.7639

The error matrix shows the biggest confusion between “Sparse Vegetation” (*Class 4*) and “Dense Vegetation” (*Class 5*) class (Table 12).

CLASS	1	2	3	4	5	TOTAL
1	1514	19	13	14	3	1563
2	0	1670	0	0	0	1670
3	27	81	2855	59	41	3063
4	12	2	317	4393	726	5450
5	2	40	6	15	6494	6557
TOTAL	1305	1812	3441	4381	7264	18203

Table 12: Confusion Matrix (September 2019)

OA [%]	88.1144
Kappa	0.7658

Based on the contingency table of the classification of the scenes from 2020 (Table 13 and 14), the largest number of pixels was assigned wrongly between the “Sparse Vegetation” (*Class 4*) and “Dense Vegetation” (*Class 5*) classes.

CLASS	1	2	3	4	5	TOTAL
1	4890	29	6	0	88	5013
2	0	1783	0	0	0	1783
3	72	0	2984	72	55	3183
4	137	0	396	4215	105	4853
5	2	0	55	94	7016	7167
TOTAL	5101	1812	3441	4381	7264	21999

Table 13: Confusion Matrix (March 2020)

OA [%]	90.1861
Kappa	0.8171

CLASS	1	2	3	4	5	TOTAL
1	1603	43	6	0	0	1652
2	0	1729	0	0	0	1729
3	45	12	3303	94	33	3487
4	4	0	56	3581	126	3767
5	0	28	76	706	7105	7915
TOTAL	1652	1812	3441	4381	7264	18550

Table 14: Confusion Matrix (August 2020)

OA [%]	85.5991
Kappa	0.7347

3.2 Temporal Development Results

The results of the previously computed statistics were depicted in graphs to create a better figure of the acquired results. The graphs were made for individual indices.

At first, graphs that represented the temporal development of the ARVI, NDVI, NBR, and dNBR values were created in such a way that the beginnings of the detection coincide for all fires, regardless of the exact date of the first detection.

Afterward, the percentual improvement over time of the values of each index was computed and depicted in graphs. The only exception where the percentual improvement could not have been computed was the *Sclerophyllous vegetation*. The first detection of this burnt area is from the November 2015 scene, so these values could not have been compared to any other scene. No other scenes from the fall were available since the Sentinel-2A satellite was launched in 2015 and Sentinel-2B in 2017.

3.2.1 Transitional woodland-shrub

While creating the graphs of temporal development for this type of forest, only mean values and standard deviation were used. The reason for this was to ensure the clarity of the graphs. Since eleven areas affected by fire in this type of forest were detected, depicting all of the values in graphs would not be reasonable because it would become difficult to understand.

ARVI Index:

The graphs show ARVI mean values of the Transitional woodland-shrub class comparing burnt and untouched areas at Fig. 25. The ARVI standard deviations are presented at Fig. 26.

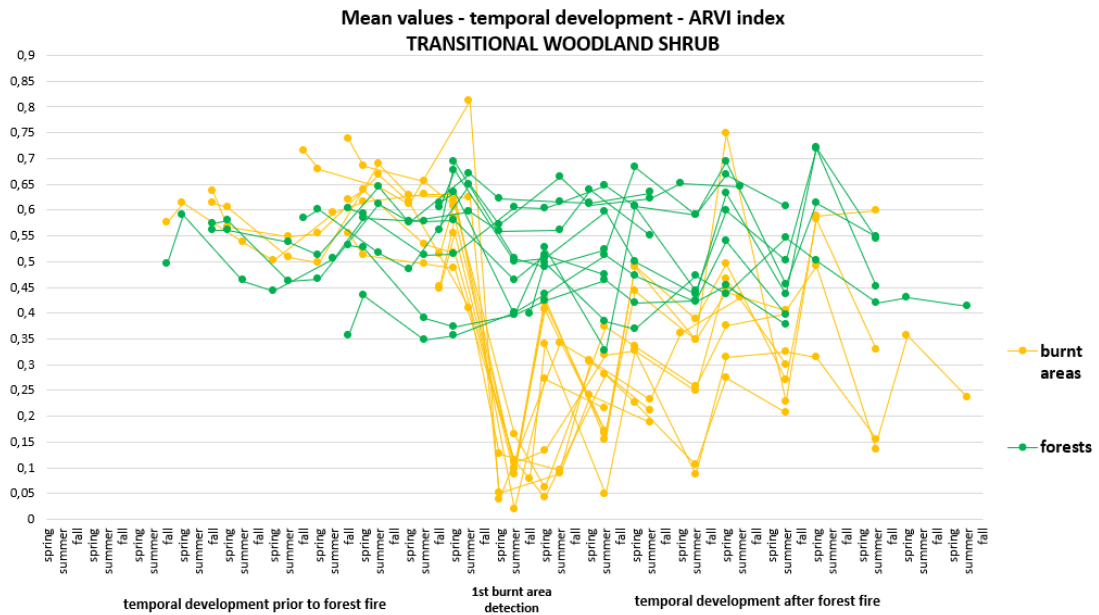


Figure 25: Transitional woodland-shrub: Temporal development of mean values - ARVI

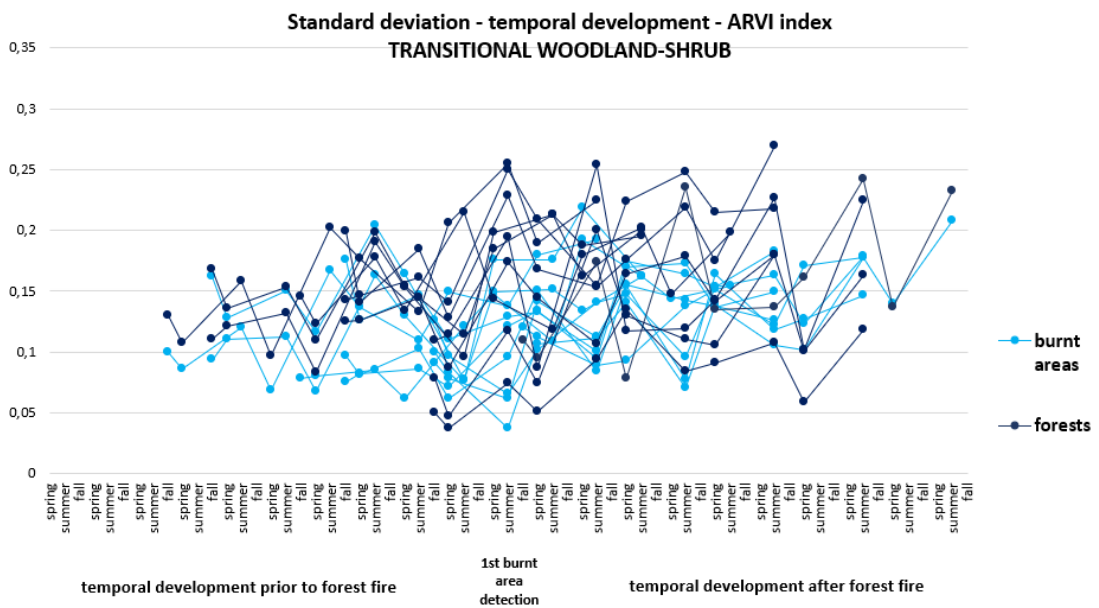


Figure 26: Transitional woodland-shrub: Temporal development of standard deviation – ARVI

Eleven homogenous test areas were collected in order to follow up the spectral evolution of the burnt areas and forested areas. It can be observed that in the case of the burnt areas' temporal development using ARVI, mean values rapidly declined in the period of the first detection. Regarding the evolution of the burnt areas with time, it is clear that the values did not increase constantly in most of the cases. While comparing the temporal development, it is necessary to separately compare summer

periods, fall periods, and spring periods with each other because of the different vegetation phases. As seen, the values of the previously burnt areas are lower in summer than in spring. It also depends on in which month the satellite data was acquired.

The graph (Fig.26) depicting the standard deviation shows that the values were not appreciably deviated from the average value even in the case of the burnt areas' development. The values representing the burnt areas were lower than for forested areas, which is predictable because the other values should not have differed from the average value by a lot.

NDVI Index:

In the case of the NDVI index, the mean values (Fig.27) showing regrowth had a smoother change of development and varied between 0.12 and 0.63. However, the ARVI shows values varied between 0.025 and 0.75 (Fig.25).

As in the previous case, the values of post-fire development of burnt areas were lower in the summer periods. The values in the period of the first detection were higher than in the case of ARVI, however, this index also showed great visibility of the regrowth after the fire. The standard deviation of NDVI also shows smoother development varying between 0.04 and 0.23 at Fig. 28 than the ARVI index (Fig. 26) which had a range of 0.035 and 0.28.

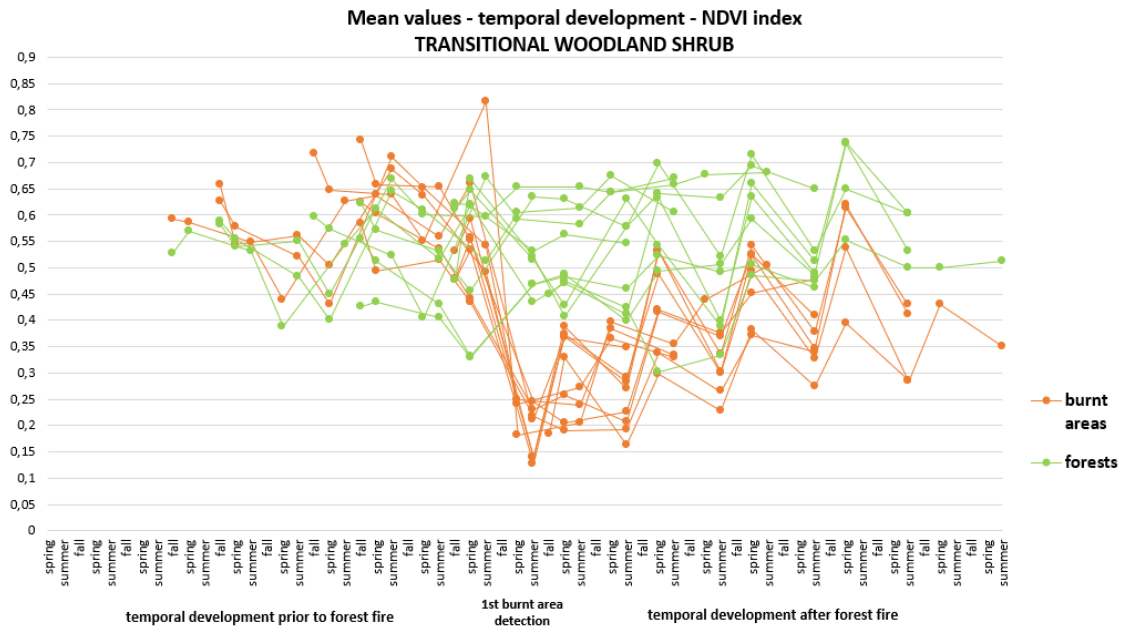


Figure 27: Transitional woodland-shrub: Temporal development of mean values - NDVI

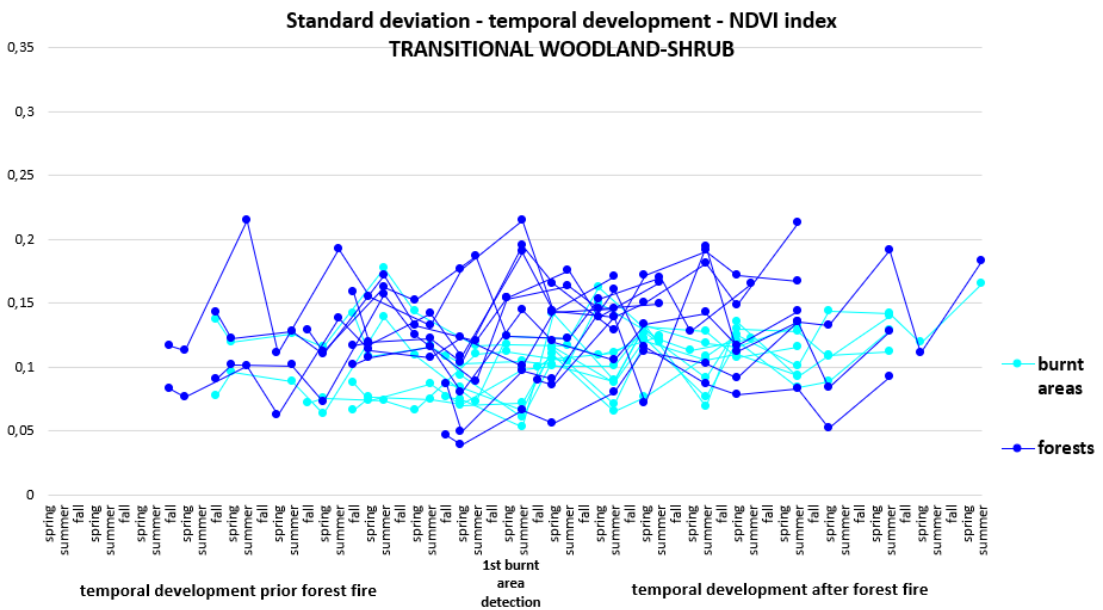


Figure 28: Transitional woodland-shrub: Temporal development of standard deviation – NDVI

NBR Index:

The NBR index (Fig. 29) indicates lower values for the burnt areas’ development mainly in the period of the first detection and after the fire. This index is used mainly for burnt area detection and the reason is clear. As in the rest of the indices, the values

for the burnt areas are much lower than the ones showing the development of the forested areas outside of the burnt areas. In the case of NBR, the mean values in the first period of the detection were negative. These values are more or less constant in all displayed areas.

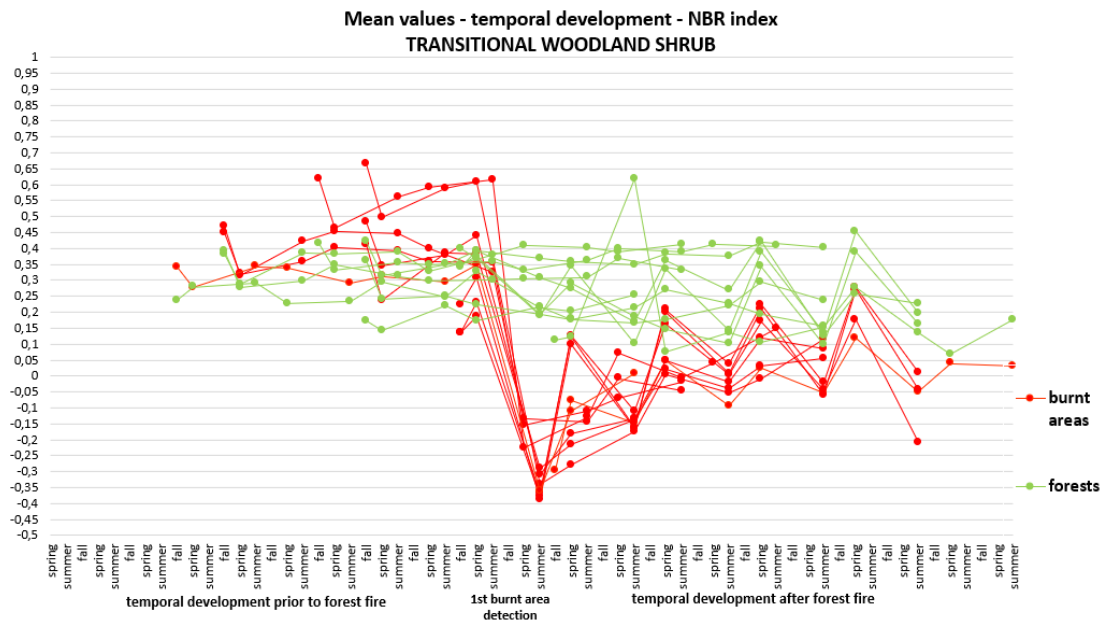


Figure 29: Transitional woodland-shrub: Temporal development of mean values - NBR

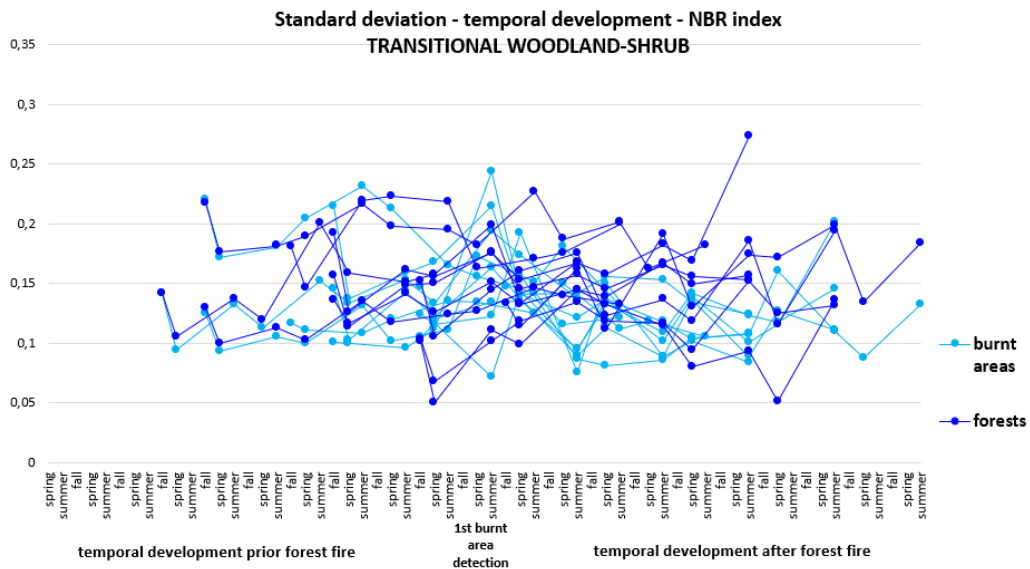


Figure 30: Transitional woodland-shrub: Temporal development of standard deviation – NBR

dNBR Index:

These graphs (Fig. 31 and 32) show the differenced NBR images. In the case of the differenced images pre and post the fires, dNBR displayed very high values that were not dependent on the order of differencing of the images. The following development depended on the order (a *summer-spring* image showed lower values, *spring-summer* image showed higher values). However, while comparing the matching order differenced images, constantly increasing values were visible.

The range of standard deviation of burnt areas in the case of dNBR is higher as seen in Fig. 32. The range is between 0.048 and 0.28.

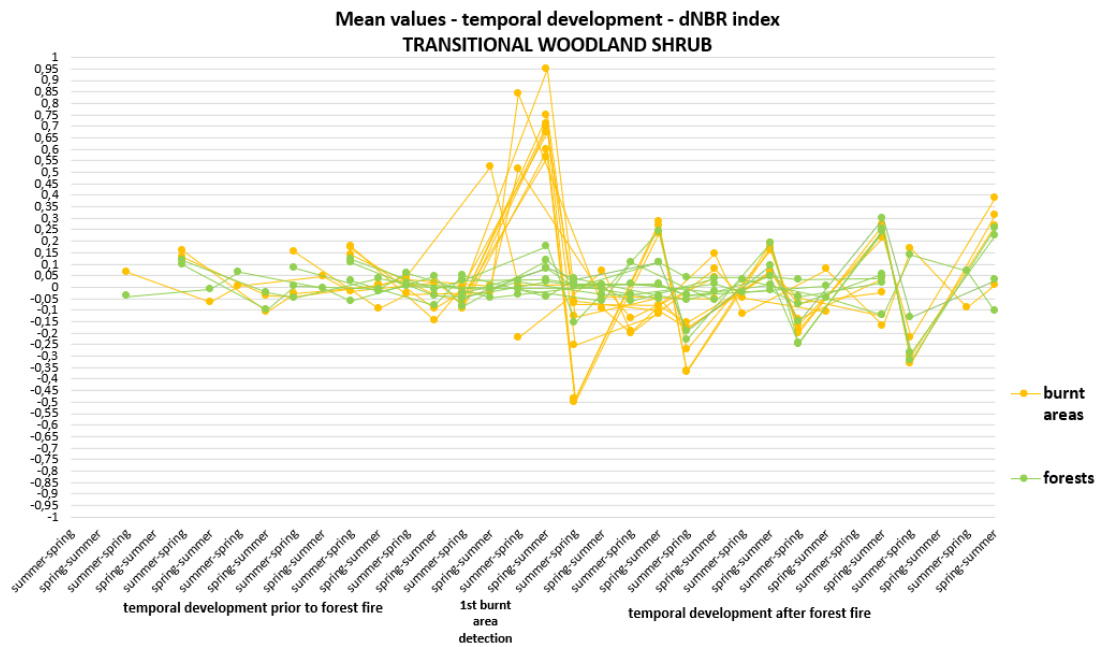


Figure 31: Transitional woodland-shrub: Temporal development of mean values - dNBR

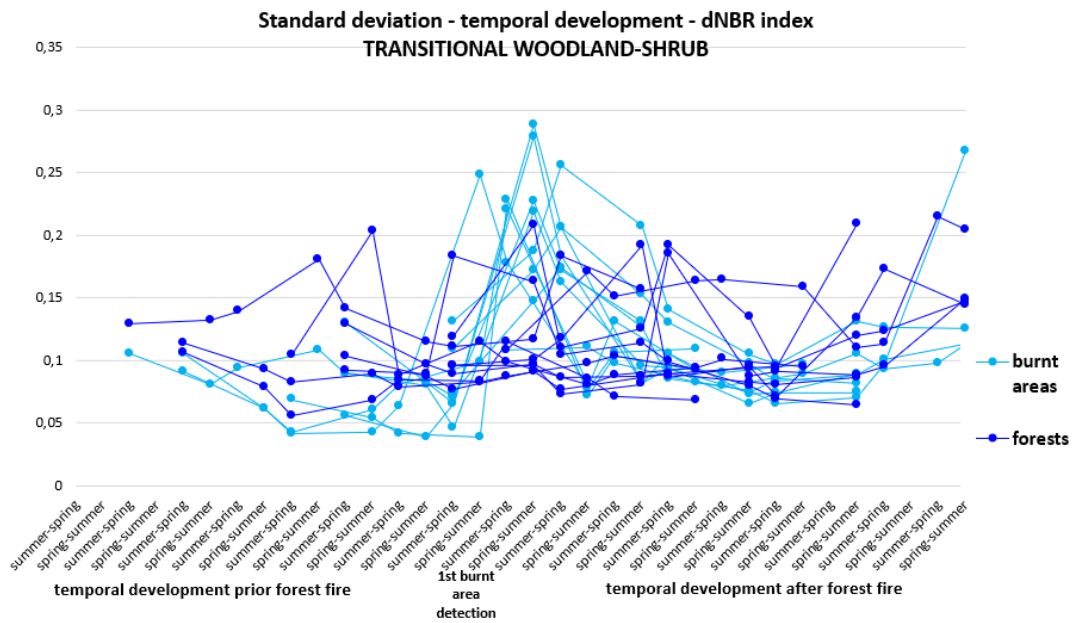


Figure 32: Transitional woodland-shrub: Temporal development of standard deviation – dNBR

In the following tables and graphs, the percentual development of the burnt areas for each index is shown. The values' development is shown based on the period of the first detection – summer/spring. Two tables (Table 15 and Table 16) and two graphs (Fig. 33 and Fig.34) in total were created for this type of forested area. The percentual development was computed for mean values and standard deviation.

Summer period – mean values of the burnt areas:

		Temporal development in % (towards the first detection)					
		Area 1	Area 2	Area 3	Area 4	Area 5	Area 6
ARVI	Pre-fire values	0.5149	0.4513	0.4458	0.5549	0.6188	0.7378
	Year after first detection						
	1st	155	55	95	147	194	128
	2nd	110	290	300	170	312	118
	3rd	132	171	367	258	359	144
	4th	214	230	415			
NDVI	Pre-fire values	0.5321	0.4793	0.4771	0.5847	0.6236	0.7426
	Year after first detection						
	1st	102	93	194	62	33	33
	2nd	116	140	285	63	60	53
	3rd	148	170	288	126	77	95
	4th	194	207	361			
NBR	Pre-fire values	0.2235	0.2304	0.1880	0.4136	0.4825	0.6666
	Year after first detection						
	1st	57	56	70	53	57	49
	2nd	102	110	101	86	93	84
	3rd	153	111	112	119	127	133
	4th	162	129	155			
dNBR	Pre-fire values	-0.0829	-0.0940	-0.0521	0.0009	-0.0201	-0.0604
	Year after first detection						
	1st	61	52	58	112	111	106
	2nd	72	71	72	90	94	90
	3rd	75	75	79	103	113	95
	4th	83	77	80			

Table 15: Transitional woodland-shrub: Temporal improvement of mean values in %

This graph (Fig. 33) shows the percentual changes of the mean values over time. All of the areas have recorded significant improvement since the first burnt area's detection between 2016 and 2020. In the case of ARVI, the improvement was by several hundred percent.

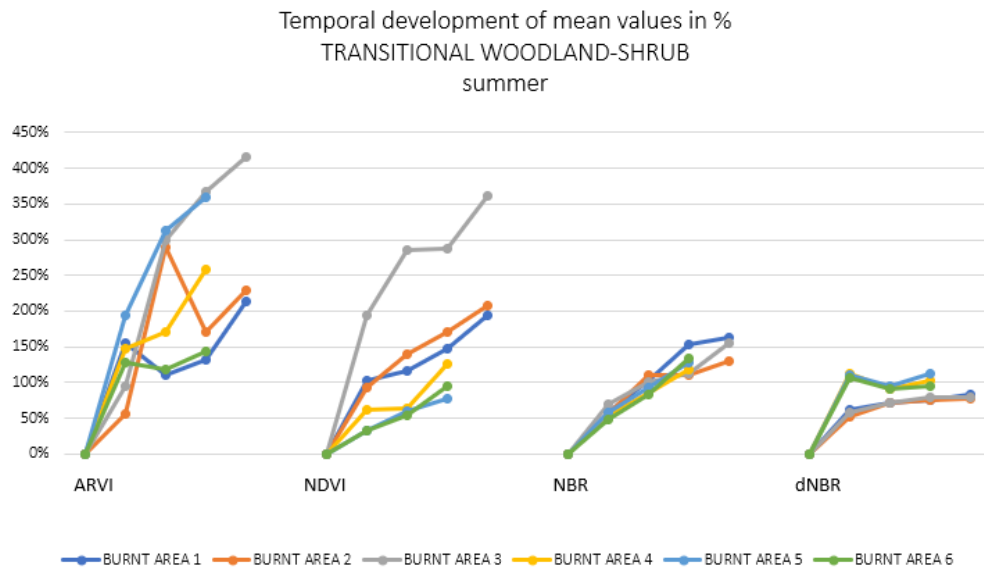


Figure 33: Transitional woodland-shrub: Temporal improvement of mean values in % - Graph

Table 16 and the following graph (Fig. 34) show that the standard deviation has also increased over time. The tables and graphs showing the development of the rest of the values (mode, median) are in *Attachment 5*.

Spring period – mean values of the burnt areas:

		Area 1	Area 2	Area 3
ARVI	Pre-fire values	0.6109	0.6272	0.6154
	Year after first detection	Temporal development in % (towards the first detection)		
	1st	294	373	142
	2nd	434		
NDVI	Pre-fire values	0.5496	0.6272	0.6377
	Year after first detection	Temporal development in % (towards the first detection)		
	1st	119	51	54
	2nd	142		
NBR	Pre-fire values	0.5917	0.3595	0.3131
	Year after first detection	Temporal development in % (towards the first detection)		
	1st	132	54	94
	2nd	119		
dNBR	Pre-fire values	-0.0231	0.0029	0.0466
	Year after first detection	Temporal development in % (towards the first detection)		
	1st	124	107	101
	2nd	105		

Table 16: Transitional woodland-shrub: Temporal improvement of standard deviation values in %

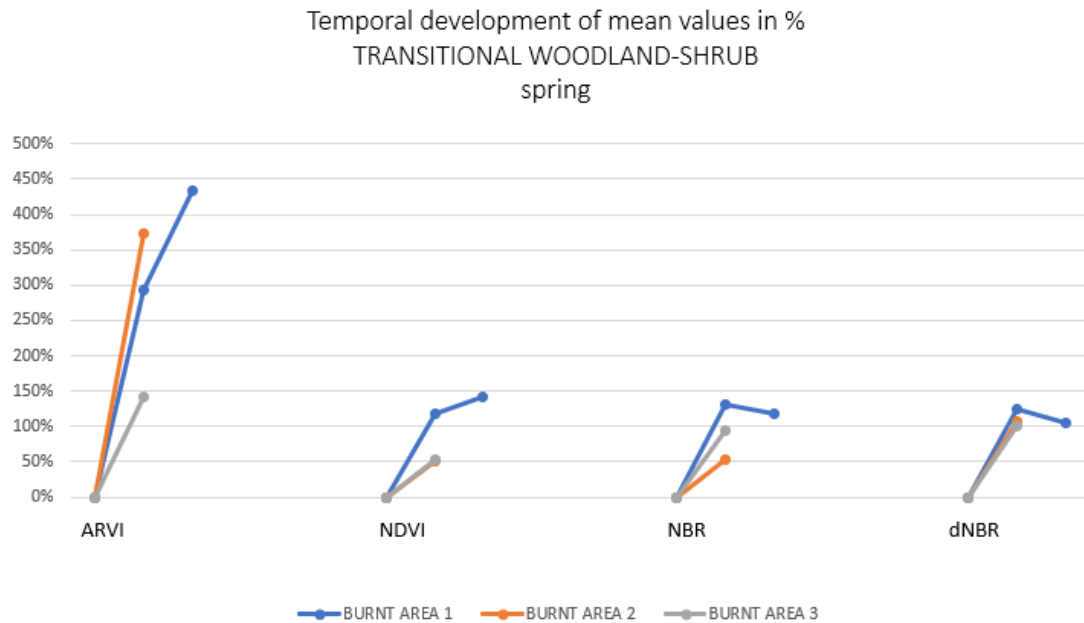


Figure 34: Transitional woodland-shrub: Temporal improvement of standard deviation values in % - Graph

3.2.2 Coniferous forests

The temporal development was depicted in four graphs. In the case of coniferous forests, only one burnt area / forested area was analyzed. The graphs (Fig. 35, 36, 37, 38) show the temporal development of mean value, standard deviation, modal value, and median for each index.

ARVI Index:

In the period of the first detection of burnt areas (Fig. 35), the values showed low mean values, modal values, and median. The values also show regrowth of vegetation over time which has not reached the pre-forest state within four years, unlike the transitional woodland-shrub area.

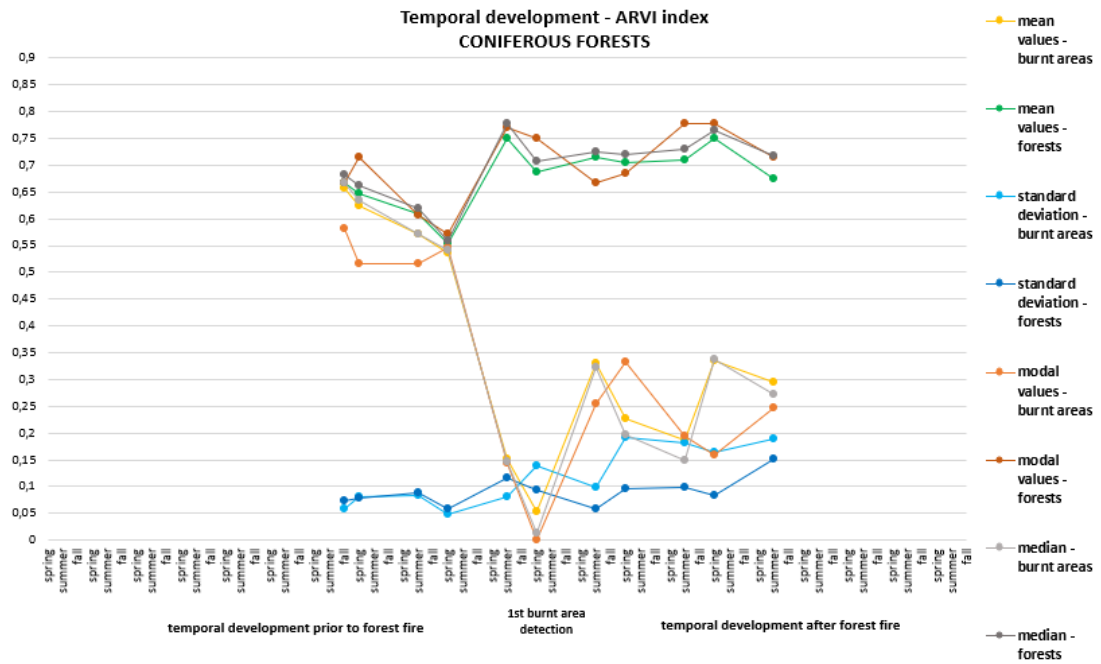


Figure 35: Coniferous Forests: Temporal development – ARVI

NDVI Index:

NDVI values (Fig. 36) show a similar trend and confirm that the recovery of the forest takes longer than in the case of transitional woodland-shrub since the final calculated NDVI values have not reached the pre-forest NDVI values in two years.

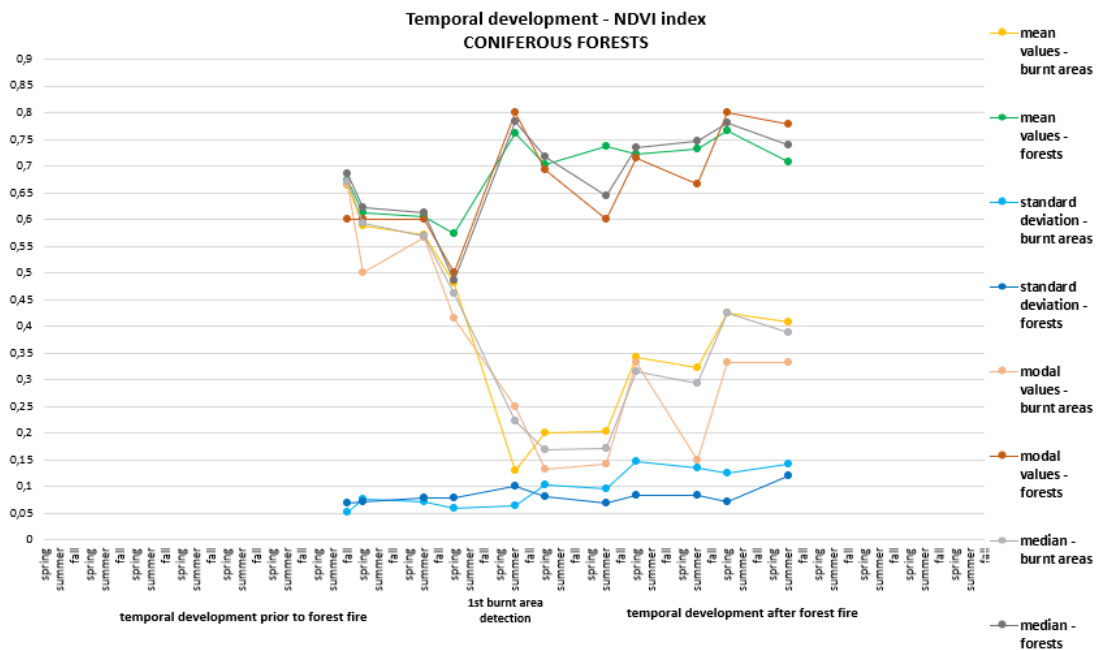


Figure 36: Coniferous Forests: Temporal development – NDVI

NBR Index:

As well as in the previous results, the increase of the NBR mean, median and modal values (Fig. 37) after the fire is recognizable. The values for the forested area show an almost constant trend. However, they have not reached the pre-fire NBR state in four years.

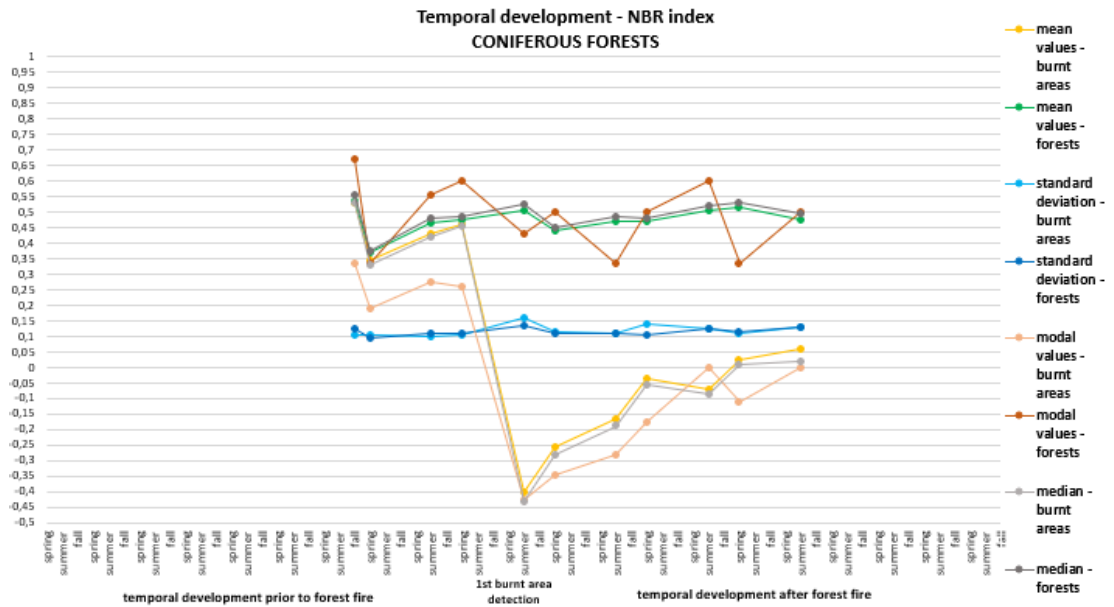


Figure 37: Coniferous Forests: Temporal development – NBR

dNBR Index:

This graph (Fig. 38) also shows the development clearly. The mean value, modal value and median faced a significant decrease of mean, mode, and median values in the period of the first detection of the burnt area. Standard deviation did not show a lot of changes over the analyzed time.

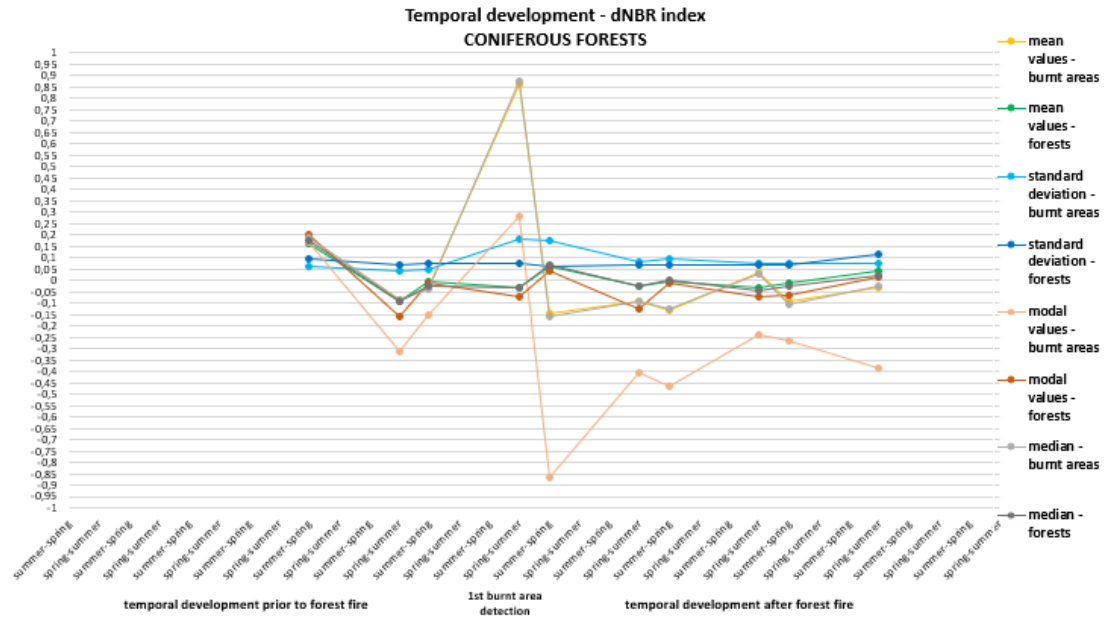


Figure 38: Coniferous Forests: Temporal development – dNBR

After that, for each index, percentual improvement of mean values, standard deviation, modal values, and median was calculated (Table 17).

		mean	st.dev	mode	median
ARVI	Pre-fire values	0.5721	0.0834	0.5169	0.5720
	Year after first detection	Temporal development in % (towards the first detection)			
	1st	79	21	78	118
	2nd	89	126	36	75
	3rd	96	135	72	85
NDVI	Pre-fire values	0.5720	0.0711	0.565	0.5691
	Year after first detection	Temporal development in % (towards the first detection)			
	1st	56	48	43	22
	2nd	148	108	40	31
	3rd	213	121	33	74
	Pre-fire values	0.4275	0.0999	0.2734	0.4158
NBR	Year after first detection	Temporal development in % (towards the first detection)			
	1st	59	33	34	56
	2nd	82	23	100	80
	3rd	114	18	100	105
dNBR	Pre-fire values	-0.03093	0.0486	-0.1498	-0.0383
	Year after first detection	Temporal development in % (towards the first detection)			
	1st	89	53	44	111
	2nd	96	58	185	96
	3rd	104	58	237	103

Table 17: Coniferous Forests: Temporal improvement of values in %

The percentual improvement over time has been quite constant (Fig.39) as well as in the case of transitional woodland-shrub. The greatest improvement of mean value was registered in the NDVI. The summer value of the burnt area has improved by more than 200% in 3 years. The biggest increase of summer modal value is shown in the dNBR.

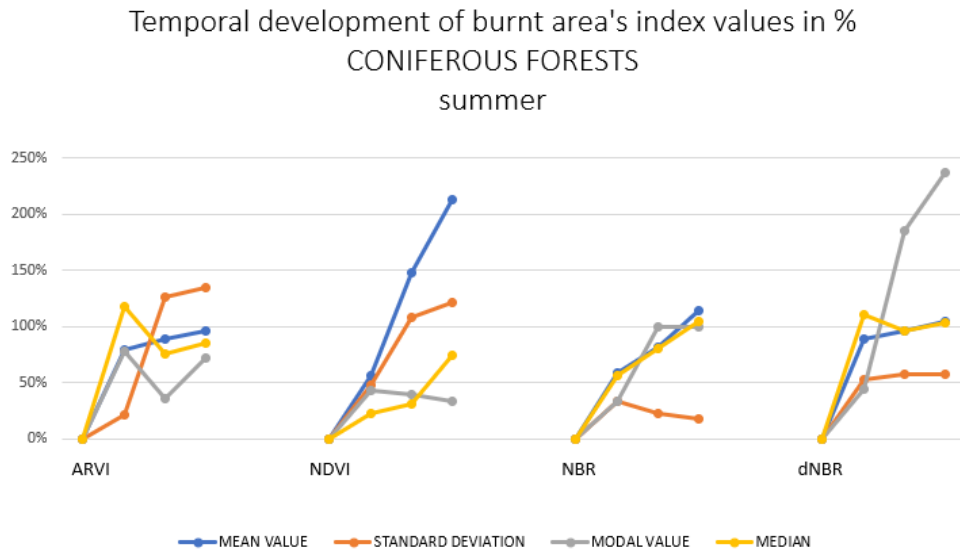


Figure 39: Coniferous Forests: Temporal improvement in % - Graph

3.2.3 Mixed Forests

In this part, the graphs and tables are displayed. The values acquired from four areas (two burnt, two forested) are described.

ARVI Index:

In the case of mixed forests, the increase of the modal values (Fig. 40) is not smooth as in the previous cases. The mean values do show a monotonous increase in the post-fire period as in the other types of forests.

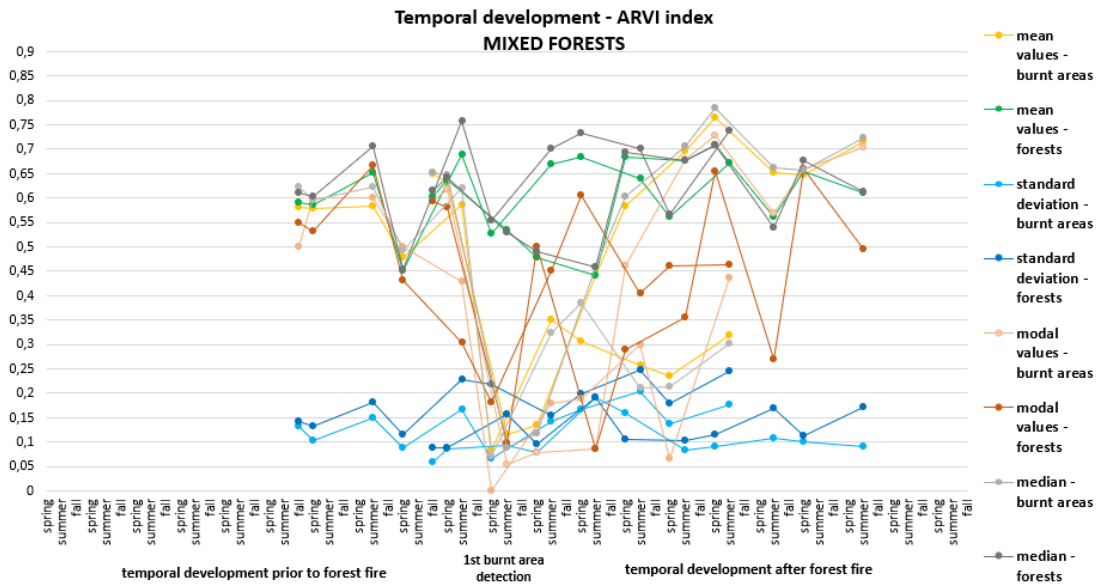


Figure 40: Mixed Forests: Temporal development – ARVI

NDVI Index:

In the case of NDVI (Fig. 41). the minimum modal value is not as low as in the case of the ARVI (Fig. 40). In the case of ARVI. the range of modal values is between 0 and 0.75. The range of the modal values in NDVI is between 0.05 and 0.8.

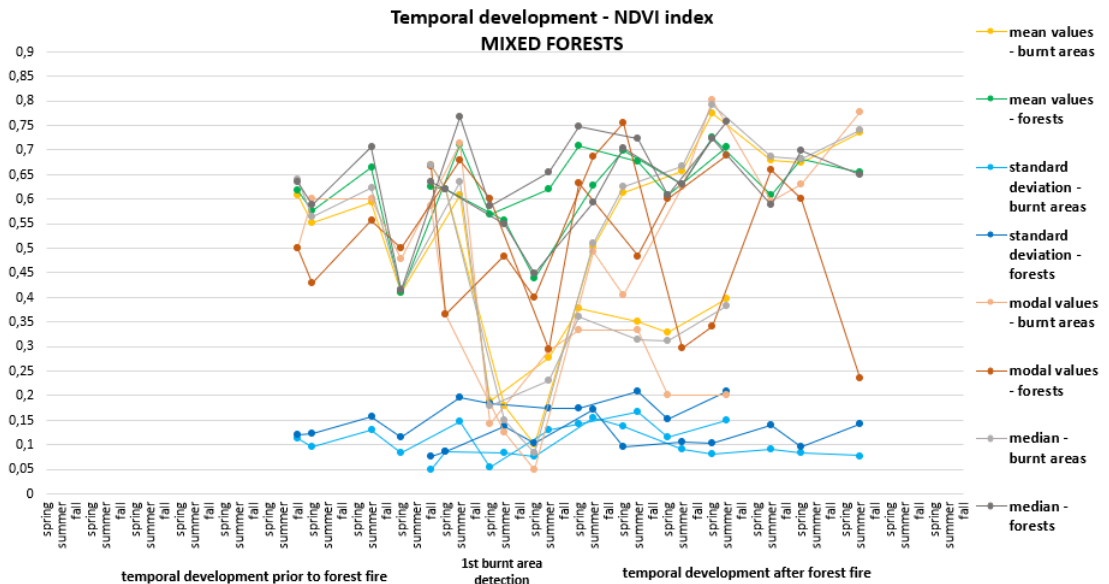


Figure 41: Mixed Forests: Temporal development – NDVI

NBR Index:

The median and mean values (Fig. 42) show the different ranges of mode and mean NBR values for comparison with NDVI (Fig. 41) and ARVI (Fig. 40). The improvement of values in NBR is slower than in the other indices as depicted in Fig. 44.

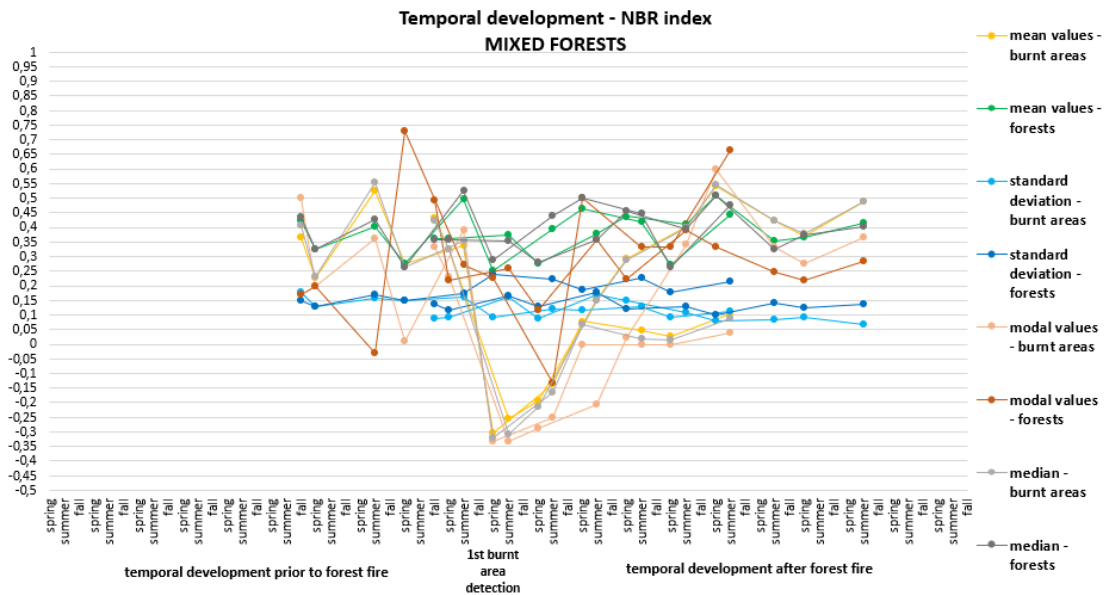


Figure 42: Mixed Forests: Temporal development – NBR

dNBR Index:

The modal values (Fig. 43). both in the burnt and untouched areas. show a different trend than in the other types of forests. Nevertheless. the mean values and median were very high in the period before the first detection.

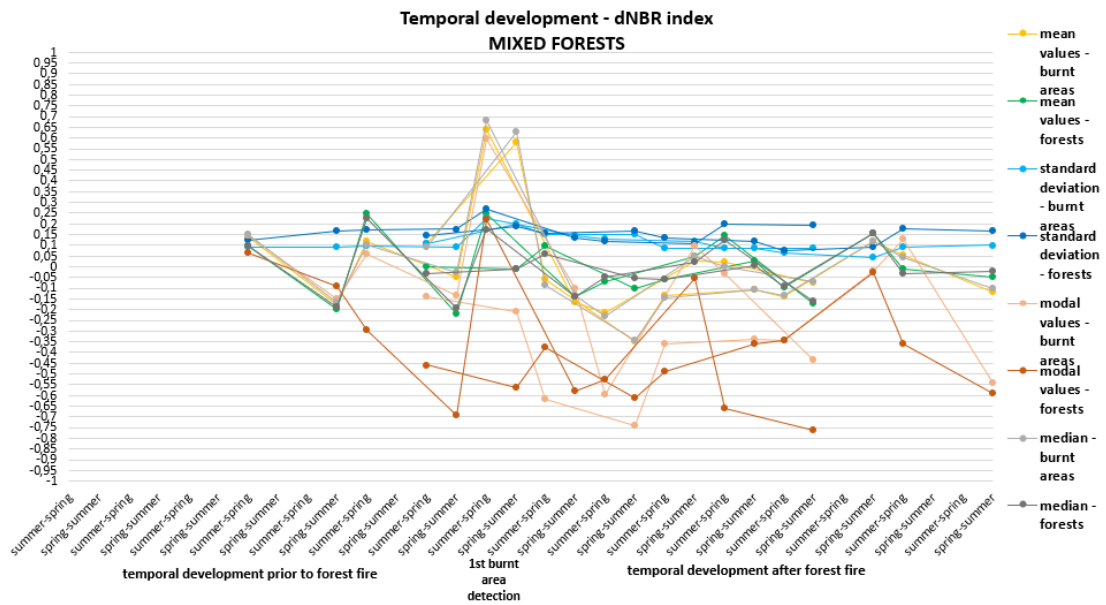


Figure 43: Mixed Forests: Temporal development – dNBR

The improvement over time as follows:

Summer period – temporal improvement:

		mean	st.dev	mode	median
		Pre-fire values	0.6487	0.0580	0.5919
ARVI	Year after first detection	Temporal development in % (towards the first detection)			
	1st	282	109	60	218
	2nd	301	10	171	300
	3rd	315	15	262	350
	4th	417	2	284	418
NDVI	Pre-fire values	0.6692	0.0486	0.5850	0.6695
	Year after first detection	Temporal development in % (towards the first detection)			
	1st	182	86	291	240
	2nd	269	9	396	345
	3rd	281	7	373	358
	4th	312	8	418	393

NBR					
	Pre-fire values	0.4323	0.0880	0.3333	0.4232
	Year after first detection	Temporal development in % (towards the first detection)			
	1st	161	5	37	148
	2nd	258	34	202	229
	3rd	267	49	200	237
	4th	293	58	210	222
dNBR					
	Pre-fire values	0.4232	0.105	-0.1373	0.0892
	Year after first detection	Temporal development in % (towards the first detection)			
	1st	100	26	51	154
	2nd	118	58	60	117
	3rd	120	78	90	81
	4th	120	51	158	116

Table 18: Mixed Forests: Temporal improvement of values in %

The most noticeable increase of the mean values was recorded in the ARVI index (Table 18 and Fig. 44). It increased by almost 420% in four years. Another significant increase was shown in the NDVI.

Temporal development of burnt area's index values in %
MIXED FORESTS
summer

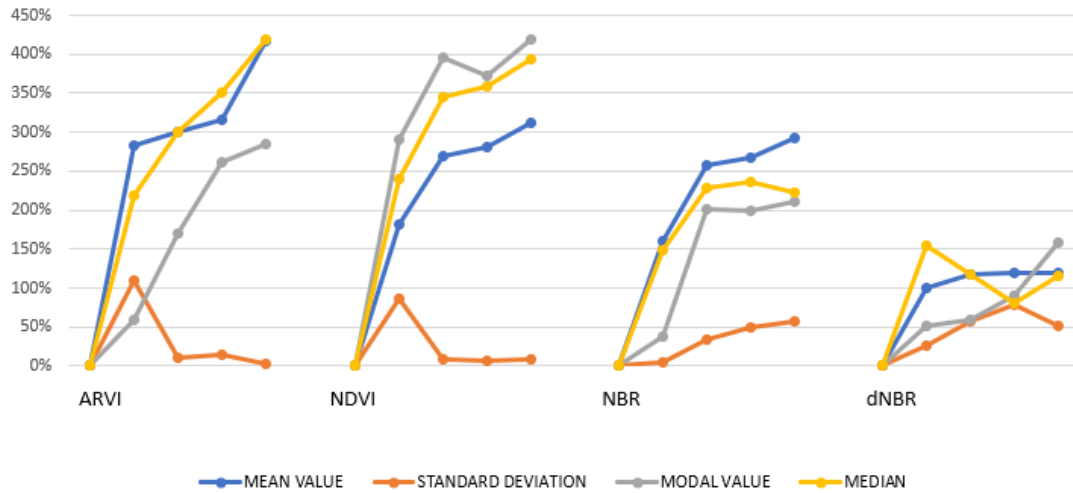


Figure 44: Mixed Forests: Temporal improvement in % - Graph

Spring period – temporal improvement:

		mean	st.dev	mode	median
		ARVI			
	Pre-fire values	0.47664	0.0874	0.5000	0.4932
	Year after first detection	Temporal development in % (towards the first detection)			
	1st	226	150	89	434
	2nd	182	105	33	196
NDVI					
	Pre-fire values	0.4089	0.0825	0.4770	0.4170
	Year after first detection	Temporal development in % (towards the first detection)			
	1st	100	160	133	100
	2nd	74	113	40	74
NBR					
	Pre-fire values	0.276	0.1472	0.0101	0.2622
	Year after first detection	Temporal development in % (towards the first detection)			
	1st	125	27	100	121
	2nd	109	0	100	105

dNBR	Pre-fire values	-0.0503	0.0895	-0.1366	-0.0291
	Year after first detection	Temporal development in % (towards the first detection)			
	1st	133	42	200	134
	2nd	96	62	105	100

Table 19: Mixed Forests: Temporal improvement of values in %

Temporal development of burnt area's index values in %
MIXED FORESTS
spring

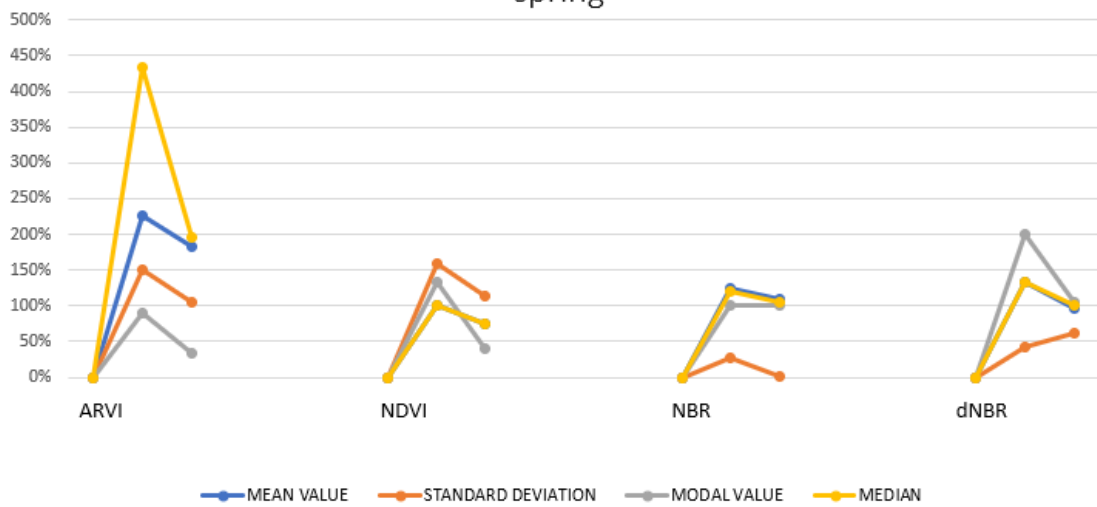


Figure 45: Mixed Forests: Temporal improvement in % - Graph

From the values and graph (Fig. 45). the percentual improvement after the first year was higher than in the second year after the detection in all the cases. The highest increase at all was observed in ARVI.

3.2.4 Sclerophyllous Vegetation

In this chapter, only the temporal development of all values is shown. The burnt area in sclerophyllous vegetation was classified in the scene from November 2015. The temporal development before the fire event was not available, so Fig. 46, 47, 48, and 49 show only the development after the burnt area was detected.

ARVI Index:

Fig. 46 shows by comparison of burnt areas and healthy forest that the decrease in the post-fire development in burnt areas was caused by other reasons than the natural post-fire development, since this decrease of modal values appears also in the healthy forest – see spring of the 4th and 5th year.

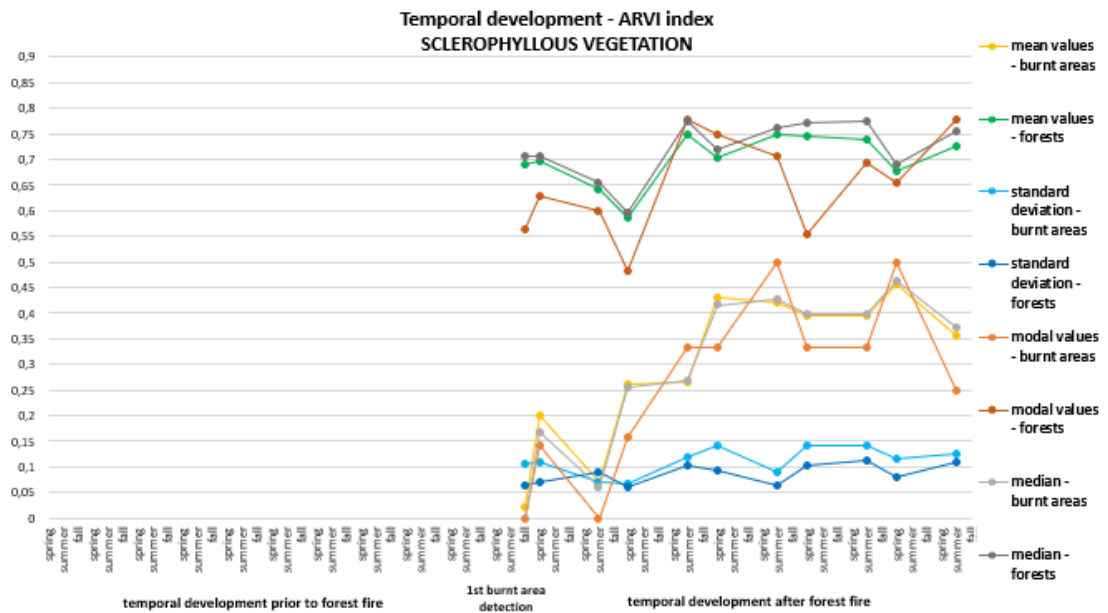


Figure 46: Sclerophyllous Vegetation: Temporal development – ARVI

NDVI Index:

The NDVI (Fig. 47) shows an almost identical trend of the development of the median and mean value of the burnt area. The same trend is visible in the case of a healthy forest.

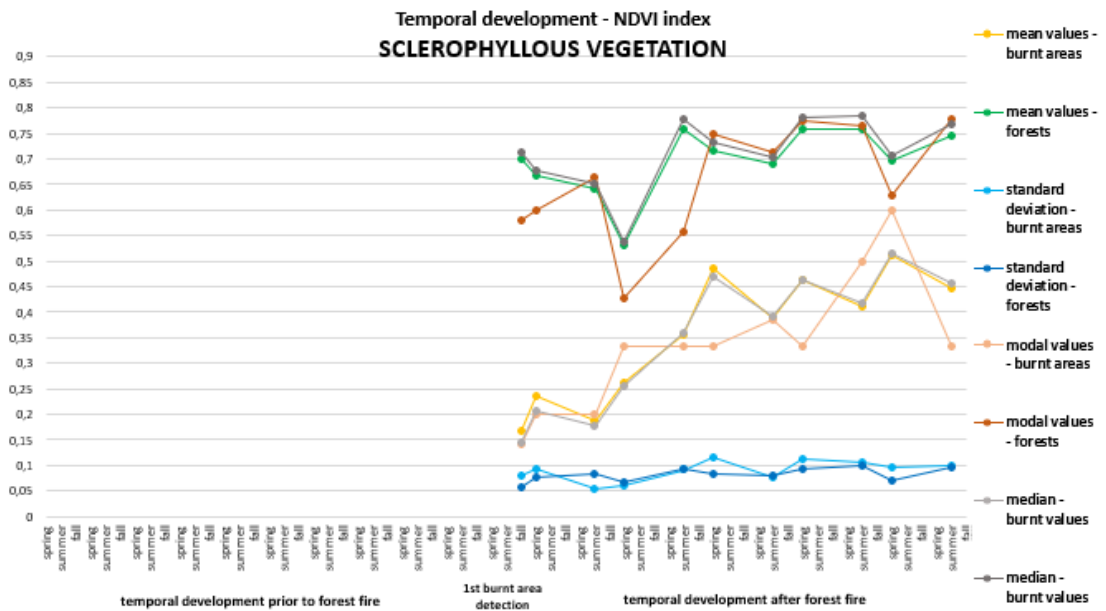


Figure 47: Sclerophyllous Vegetation: Temporal development – NDVI

NBR Index:

The NBR (Fig. 48) also shows increasing modal values in a forested area in the 4th summer period. The mean values of the burnt area are increasing.

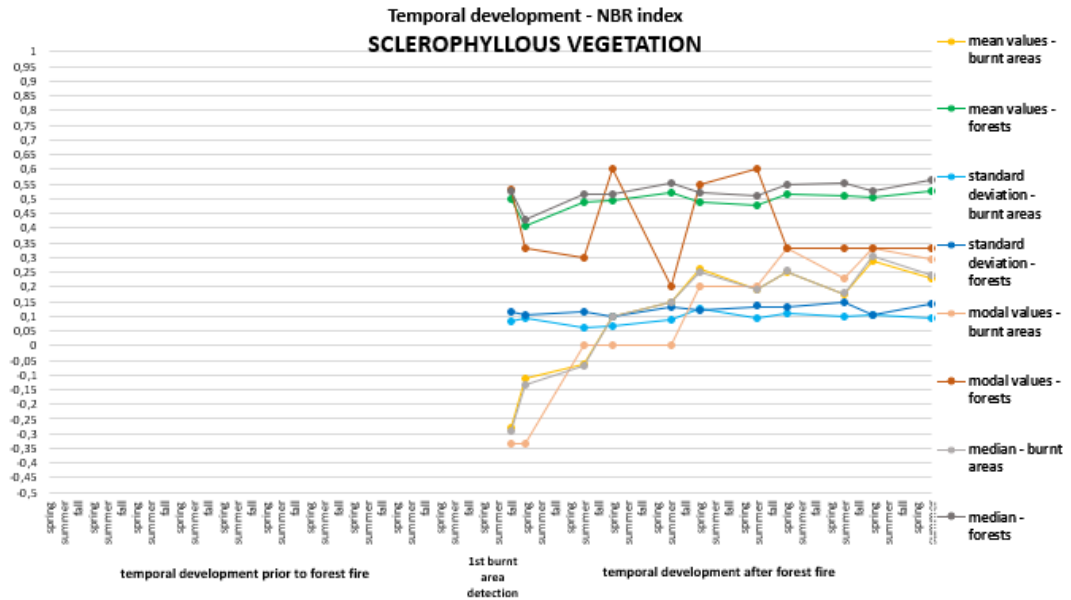


Figure 48: Sclerophyllous Vegetation: Temporal development – NBR

dNBR Index:

The pre-fire image was not available. The values of the burnt area of differenced NBR images in the years after the fire are lower than in the forested area. However, the progress of the areas is distinguishable from Fig. 49.

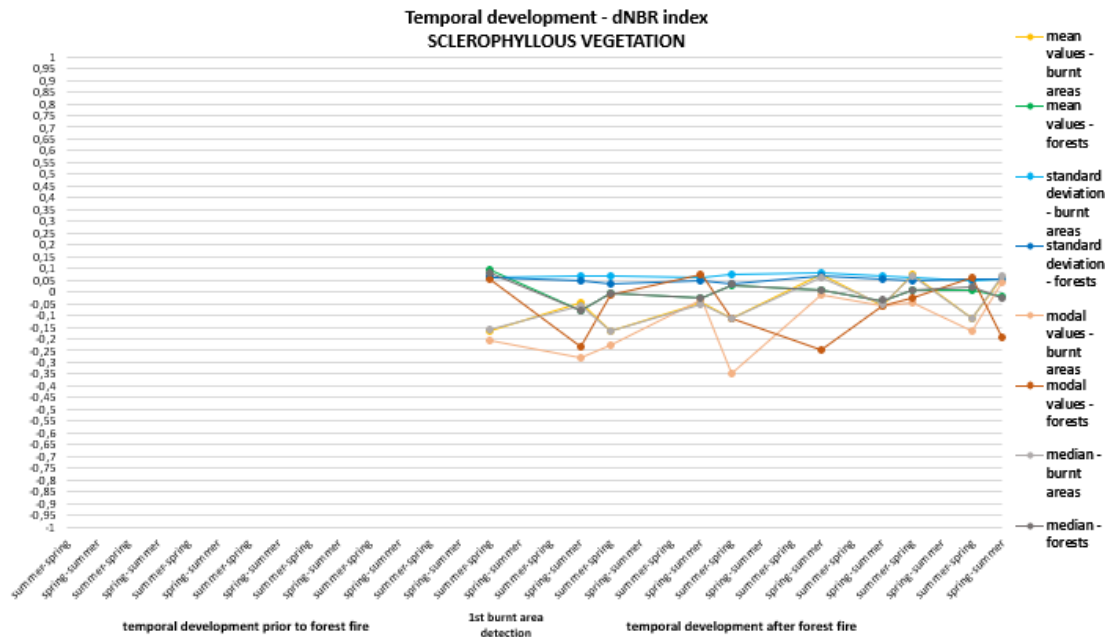


Figure 49: Sclerophyllous Vegetation: Temporal development – dNBR

In all vegetation indices (Fig. 46. 47. 48. 49). the regeneration (regrowth) of the burnt area is visible. The mean, modal and median values showed the lowest values in the period of the first detection. The values have been increasing since then. All the values of the untouched forested areas and the burnt areas are very close to each other, more than in other classes. It can be deduced that either the severity of the burnt areas is lower than in other classes or the regeneration of the forested areas is more rapid.

Discussion

The results of this thesis are in line with the hypothesis that the vegetation indices (NDVI, ARVI, NBR, dNBR) could be used for the pre and post-fire analysis. The results corresponded with the claims of *Barbosa, Caerano, and Santos, 2000* that the spectral changes of the terrain after a fire could have been analyzed using ARVI. The other two indices, NDVI and NBR, turned out to be another great possibility for the pre and post-fire temporal analysis, which had been mentioned in the study of *Gibson, Danaher, Hehir, Collins, 2020*. All three of these indices (plus dNBR) were used in the study, however, modifications of the workflow were necessary. For the execution of the classification, another ten spectral bands were added to the ground truth raster. It was one of the important modifications. Another modification was the computation of the dNBR from two consecutive scenes to depict the development in graphs.

These results should be taken into account when considering how to quite easily carry out the temporal pre and post-fire analysis of the forested areas. One of the greatest perks of this workflow is that the study can be applied for the analysis of larger areas, such as the area of the Sentinel-2 scenes. The researched studies have always analyzed smaller areas of interest than in the case of this thesis.

Due to the unavailability of the cloudless scene from summer 2015, the classification had to be executed for the image from fall 2015. It could be considered as one of the limitations of the study, because all of the other scenes were acquired in summer. It meant that the percentual improvement (regrowth) of the burnt areas classified from the 2015 scene could not have been carried out. However, not many problems were faced during the processing itself.

In the future, the same workflow could be applied using SAVI (Soil-adjusted Vegetation Index) as well as the other indices. SAVI was tested in the study focusing on fire severity and post fire regeneration (*Tonbul, Kavzoglu and Kaya, 2016*). Future studies could also take into account another type of classification or another type of classifier.

Conclusion

This thesis aimed to select the area regarding its frequency and severity of forest fires. to determine the selection of the seasons and years for future analysis. to find a suitable methodology according to the research. to compare the classified burnt areas with the CLC Burnt Area class. and to evaluate the temporal development in the various types of forested areas. All of these goals were met successfully.

The results indicated that the burnt areas had been detected from the Sentinel-2 data for almost three years. The longest period of burnt area detection by classification was observed in the transitional woodland-shrub vegetation type. The study demonstrated that the supervised classification using the Maximum Likelihood classifier could have been one of the methods for detecting the burnt areas from the satellite data. The comparison of the classified burnt area and CLC Burnt Area class showed a lot of discrepancy. Most of the classified burnt areas from all eleven scenes (from 2015 to 2020) were not included in the CLC. The analysis of the temporal development of the burnt areas in all types of forests supported the theory that the regeneration had been gradual. In several burnt areas. the mean. modal or median values of the indices showed the regrowth of the vegetation by almost 450% in three years. Also. the temporal development demonstrated significantly decreasing index values in the scenes acquired immediately (in a few-months period) after the fire had broken out.

The classification was carried out for all eleven scenes (between 2015 fall and 2020 summer). The spectral indices NDVI. ARVI. and NBR were used as additional bands for the classification. Five classes based on their spectral signatures were defined and the classification using Maximum Likelihood classifier was performed in QGIS. The classification's accuracy of all scenes was > 85%.

The classified burnt areas were compared to the CLC Burnt Area class and analyzed the concordances and differences between the classified burnt areas and CLC Burnt Areas class. It was discovered that a lot of the classified burnt areas are not depicted in the CLC Burnt Area class. from neither 2012 nor 2018.

Four types of forested areas were distinguished – *transitional woodland-shrub*. *coniferous forests*. *mixed forests*. and *sclerophyllous vegetation*. After the

classification. the burnt areas were divided according to the type of forests. in which they occurred.

Mean values, modal values, median, and standard deviation were computed using the *Zonal Statistic* function in QGIS. The temporal analysis of the burnt areas caused by the fire events in the types of forests mentioned above was executed and the graphs showing the evolution were created. The analysis showed the increase of the indices' values, which indicated the gradual regeneration of the burnt areas. Post-fire ARVI mean values and medians of transitional woodland-shrub and mixed forests showed relatively rapid regeneration compared with other indices. However, the greatest percentual improvement of mean values in burnt coniferous forests was observed in NDVI. The highest median and modal values were in dNBR while comparing with other indices. Based on the results of the percentual improvement, the most rapid regeneration is shown in the mixed forests. The post-fire temporal development of the sclerophyllous vegetation also showed a significant improvement, however, the percentual development is not available.

To conclude, the study showed a suitable option for carrying out the temporal analysis of the burnt areas. It could be used as a base for future studies focusing on pre and post-fire analysis applied to satellite data. The CORINE data do not allow to detect all of the burnt areas in Europe due to long period (2012 – 2018) between CORINE data, and due to a necessary level of the forest damage/recovery after the fire, which is determined by the CORINE Class definition for burnt areas.

References

- [1] Initiation fund of the Faculty of Civil Engineering CTU [Online]. [2021-03-17]. Available at: <https://web.fsv.cvut.cz/aktuality/490/>
- [2] BARBOSA M.. Paulo; CAETANO R.. Mário; SANTOS G.. Teresa. *Detection of changes in forest landcover type after fires in Portugal*. ISPRS Archives 2000. [Online]. [2021-04-18]. Available at: https://www.isprs.org/proceedings/XXXIII/congress/part7/126_XXXIII-part7.pdf
- [3] MALLINIS. Giorgos; MITSOPOULOS. Ioannis; CHRYSAFI. Irene. *Evaluating and comparing Sentinel-2A and Landsat-8 Operational Land Imager (OLI) spectral indices for estimating fire severity in a Mediterranean pine ecosystem of Greece*. GIScience & Remote Sensing 2017. [Online]. [2021-04-18]. Available at: <https://www.tandfonline-com.ezproxy.techlib.cz/doi/full/10.1080/15481603.2017.1354803>
- [4] PATRONO. Andrea; BAPTISTA. Adriano; EBELTJES. Jan. *Multitemporal LANDSAT TM data for monitoring the effects of forest fires and vegetation recovery processes in the Mediterranean areas*. ISPRS Archives 2000. [Online]. [2021-04-18]. Available at: https://www.isprs.org/proceedings/XXXIII/congress/part7/1131_XXXIII-part7.pdf
- [5] VIEDMA. O.; MELIÁ. J.; SEGARRA D.; GARCIA-HARO J. *Modeling rates of ecosystem recovery after fires by using Landsat TM data*. Remote Sensing of Environment. Volume 61. Issue 3. September 1997. Pages 383-398.1997. [Online]. [2021-04-18]. Available at: <https://www.sciencedirect-com.ezproxy.techlib.cz/science/article/pii/S0034425797000485?via3Dihub>
- [6] GALLAUN. Heinz; BANNINGER. Cliff. *Monitoring fire – affected wildlands in the Mediterranean region by applying a remote sensing and GIS approach*. ISPRS archives 1996. [Online]. [2021-04-18]. Available at: https://www.isprs.org/proceedings/XXXI/congress/part7/240_XXXI-part7.pdf
- [7] LASAPONARA. Rosa; TUCCI. Biagio; GHERMANDI. Luciana. *On the Use of Satellite Sentinel-2 Data for Automatic Mapping of Burnt Areas and Burn Severity*.

- Sustainability 2018. [Online]. [2021-04-18]. Available at: <https://www.mdpi.com/2071-1050/10/11/3889/htm>
- [8] TONBUL. H.; KAVZOGLU T.; KAYA. S. *Assessment of Fire Severity and Post-Fire Regeneration based on Topographical Features using Multitemporal Landsat Imagery: A CASE STUDY in MERSIN. TURKEY*. ISPRS Archives 2016. [Online]. [2021-04-19]. Available at: <https://www.int-arch-photogramm-remote-sens-spatial-inf-sci.net/XLI-B8/763/2016/isprs-archives-XLI-B8-763-2016.pdf>
- [9] GIBSON. Rebecca; DANAHER. Tim; HEHIR. Warwick; COLLINS. Luke. *A Remote Sensing Approach to Mapping Fire Severity in South-Eastern Australia using Sentinel-2 and Random Forest*. Science Direct 2020. [Online]. [2021-04-19]. Available at: [https://www.sciencedirect-com.ezproxy.techlib.cz/science/article/pii/S0034425720300717?via3Dihub](https://www.sciencedirect.com.ezproxy.techlib.cz/science/article/pii/S0034425720300717?via3Dihub)
- [10] Mediterranean climate. Wikipedia. The Free Encyclopedia. [Online]. [2021-04-19]. Available at: https://en.wikipedia.org/wiki/Mediterranean_climate#Hot-summer_mediterranean_climate
- [11] European Space Agency. Sentinel-2 operations. [Online]. [2021-04-20]. Available at: https://www.esa.int/Enabling_Support/Operations/Sentinel-2_operations
- [12] European Space Agency. Product Types. Sentinel Online. [Online]. [2021-04-20]. Available at: <https://sentinels.copernicus.eu/web/sentinel/user-guides/sentinel-2-msi/product-types>
- [13] European Space Agency. Spatial resolution. Sentinel Online. [Online]. [2021-04-21]. Available at: <https://sentinel.esa.int/web/sentinel/user-guides/sentinel-2-msi/resolutions/spatial>
- [14] European Space Agency. Resolution and Swath. Sentinel Online. [Online]. [2021-04-21]. Available at: <https://sentinel.esa.int/web/sentinel/missions/sentinel-2/instrument-payload/resolution-and-swath>
- [15] United Nations. Top of the Atmosphere. [2021-04-26]. [Online]. Available at: <https://www.un-spider.org/node/10958>

- [16] Sentinel Hub. Normalized Difference Vegetation Index. [2021-04-26]. [Online]. Available at: <https://custom-scripts.sentinel-hub.com/custom-scripts/sentinel-2/ndvi/>
- [17] KAUFMAN, Y.J and TANRÉ, D. *Atmospherically resistant vegetation index (ARVI) for EOS-MODIS*. Proc. of IEEE IGARS'92. 261-270. IEEE.1992. [2021-04-26]. [Online]. Available at: <https://ieeexplore-ieee-org.ezproxy.techlib.cz/document/134076>
- [18] Corine Land Cover Classes. [Online]. [2021-05-20]. Available at: https://land.copernicus.eu/Corinelandcoverclasses.eps.75dpi.png/image_view_fullscreen
- [19] Copernicus. Updated CLC illustrated nomenclature guidelines. [2021-05-08]. [Online]. Available at: https://land.copernicus.eu/user-corner/technical-library/corine-land-cover-nomenclature-guidelines/docs/pdf/CLC2018_Nomenclature_illustrated_guide_20190510.pdf
- [20] CORINE Land Cover. Copernicus Land Monitoring Service [Online]. [2021-04-20]. Available at: <https://land.copernicus.eu/pan-european/corine-land-cover>
- [21] CORINE Land Cover. Burnt Areas Class. [Online]. [2021-04-20]. Available at: <https://land.copernicus.eu/user-corner/technical-library/corine-land-cover-nomenclature-guidelines/html/index-clc-334.html>
- [22] HALOUNOVÁ, L.. Zpracování obrazových dat. CTU Prague. 2008. ISBN: 978-80-01-04253-3
- [23] JWAN A., MANSOR S. B. and SHAFRI H. Image Classification in Remote Sensing. Journal of Environment and Earth Science. ISSN 2225-0948. Vol. 3. No.10. 2013. [2021-04-27]. [Online]. Available at: <https://core.ac.uk/download/pdf/234663192.pdf>
- [24] QGIS Documentation. Sieve. [2021-04-29]. [Online]. Available at : https://docs.qgis.org/2.8/en/docs/user_manual/processing_algs/gdalogr/gdal_analysis/sieve.html

- [25] United Nation. NBR. [2021-05-01]. [Online]. Available at: <https://un-spider.org/advisory-support/recommended-practices/recommended-practice-burn-severity/in-detail/normalized-burn-ratio>
- [26] QGIS. GISMentors. [Online]. [2021-04-21]. Available at: <https://gismentors.cz/skoleni/qgis/>
- [27] QGIS Plugins. Semi-Automatic Classification Plugin. [Online]. [2021-04-21]. Available at: <https://plugins.qgis.org/plugins/SemiAutomaticClassificationPlugin/>
- [28] GRASS GIS. General Overview. [Online]. [2021-04-21]. Available at: <https://grass.osgeo.org/learn/overview/>
- [29] Documentation QGIS. GRASS GIS Integration. [2021-04-21]. Available at: https://docs.qgis.org/2.8/en/docs/user_manual/grass_integration/grass_integration.html

List of Figures

Figure 1: Study Area.....	24
Figure 2: Wavelengths and Bandwidths of the 3 Spatial Resolutions of the MSI instruments [14].....	28
Figure 3: Sentinel-2 10 m spatial resolution bands: B2 (490 nm). B3 (560 nm). B4 (665 nm) and B8 (842 nm) [13].....	28
Figure 4: SENTINEL-2 20 m spatial resolution bands: B5 (705 nm). B6 (740 nm). B7 (783 nm). B8a (865 nm). B11 (1610 nm) and B12 (2190 nm) [13].....	29
Figure 5: SENTINEL-2 60 m spatial resolution bands: B1 (443 nm). B9 (940 nm) and B10 (1375 nm) [13].....	29
Figure 6: Sentinel-2A image of the area of interest acquired in August 2020.....	30
Figure 7: CLC Classes [18].....	36
Figure 8: Gaussian distributin. Source:Wikipedia.....	40
Figure 9: Burnt area (based on Sentinel-2 bands B8. B4. B3). Source: Sentinel Hub Playground	42
Figure 10: Scheme of the burnt areas' comparison	49
Figure 11: QGIS logo [26].....	53
Figure 12: GRASS GIS logo [28].....	54
Figure 13: Legend.....	55
Figure 14: Classified scene from November 2015.....	55
Figure 15: Classified scene from April 2016	Figure 16: Classified scene from August 2016
2016	55
Figure 17: Classified scene from March 2017	Figure 18: Classified scene from
September 2017	56
Figure 19: Classified scene from May 2018	Figure 20: Classified scene from August
2018	56
Figure 21: Classified scene from May 2019	Figure 22: Classified scene from
September 2019	56
Figure 23: Classified scene from March 2020	Figure 24: Classified scene from
August 2020	57
Figure 25: Transitional woodland-shrub: Temporal development of mean values - ARVI ..	63
Figure 26: Transitional woodland-shrub: Temporal development of standard deviation – ARVI	63
Figure 27: Transitional woodland-shrub: Temporal development of mean values - NDVI ..	65

Figure 28: Transitional woodland-shrub: Temporal development of standard deviation – NDVI	65
Figure 29: Transitional woodland-shrub: Temporal development of mean values - NBR	66
Figure 30: Transitional woodland-shrub: Temporal development of standard deviation – NBR	66
Figure 31: Transitional woodland-shrub: Temporal development of mean values - dNBR ..	67
Figure 32: Transitional woodland-shrub: Temporal development of standard deviation – dNBR	68
Figure 33: Transitional woodland-shrub: Temporal improvement of mean values in % - Graph	70
Figure 34: Transitional woodland-shrub: Temporal improvement of standard deviation values in % - Graph.....	72
Figure 35: Coniferous Forests: Temporal development – ARVI.....	73
Figure 36: Coniferous Forests: Temporal development – NDVI.....	73
Figure 37: Coniferous Forests: Temporal development – NBR	74
Figure 38: Coniferous Forests: Temporal development – dNBR	75
Figure 39: Coniferous Forests: Temporal improvement in % - Graph	77
Figure 40: Mixed Forests: Temporal development – ARVI.....	78
Figure 41: Mixed Forests: Temporal development – NDVI.....	78
Figure 42: Mixed Forests: Temporal development – NBR.....	79
Figure 43: Mixed Forests: Temporal development – dNBR.....	80
Figure 44: Mixed Forests: Temporal improvement in % - Graph	82
Figure 45: Mixed Forests: Temporal improvement in % - Graph	83
Figure 46: Sclerophyllous Vegetation: Temporal development – ARVI.....	84
Figure 47: Sclerophyllous Vegetation: Temporal development – NDVI	85
Figure 48: Sclerophyllous Vegetation: Temporal development – NBR	86
Figure 49: Sclerophyllous Vegetation: Temporal development – dNBR	87

List of Tables

Table 1: Specifications of images used in this study	31
Table 2: Classified burnt areas registered in CORINE Land Cover 2018	48
Table 3: Number of Burnt Areas in each layer	50
Table 4: Confusion Matrix (November 2015)	58
Table 5: Confusion Matrix (April 2016).....	58
Table 6: Confusion Matrix (August 2016).....	58
Table 7: Confusion Matrix (March 2017).....	59
Table 8: Confusion Matrix (September 2017)	59
Table 9: Confusion Matrix (May 2018).....	59
Table 10: Confusion Matrix (August 2018).....	60
Table 11: Confusion Matrix (May 2019).....	60
Table 12: Confusion Matrix (September 2019)	60
Table 13: Confusion Matrix (March 2020).....	61
Table 14: Confusion Matrix (August 2020).....	61
Table 15: Transitional woodland-shrub: Temporal improvement of mean values in %	69
Table 16: Transitional woodland-shrub: Temporal improvement of standard deviation values in %	71
Table 17: Coniferous Forests: Temporal improvement of values in %	76
Table 18: Mixed Forests: Temporal improvement of values in %.....	81
Table 19: Mixed Forests: Temporal improvement of values in %.....	83

Attachments

Attachment 1: Transitional Woodland-shrub – values. *.xls* (electronic)

Attachment 2: Coniferous Forests – values. *.xls* (electronic)

Attachment 3: Mixed Forests – values. *.xls* (electronic)

Attachment 4: Sclerophyllous Vegetation – values. *.xls* (electronic)

Attachment 5: Percentual Improvement – values + graphs. *.xls* (electronic)

Attachment 6: Training Sets. *.scp* (electronic)

Attachment 7: Testing Sets. *.scp* (electronic)